Department of Physics and Astronomy
University of Heidelberg

State Examination Thesis in Physics
submitted by

Nilab Abbas

born in Rendsburg (Germany)

2021

Raman Transitions with a Phase Locked Laser System

This thesis has been carried out by Nilab Abbas at the
Physikalisches Institut in Heidelberg
under the supervision of
Prof. Dr. Selim Jochim

Abstract

This thesis presents Raman transitions between two hyperfine ground states in ultracold ^{6}Li atoms with an optical phase locked loop. Raman transitions offer fast population transfer with high spatial resolution for quenching interactions, e.g. to the measure momentum distribution of an expanding atomic cloud. The crucial condition here is coherence of both light fields, relative phase noise would suppress the transition. To ensure phase stability during the experiment, an optical phase-locked loop was used, which continuously regulates one of the two lasers used such that there is a stable phase and frequency relation to the second laser. Raman transitions between ground states $|3\rangle$ and $|4\rangle$ were measured at a magnetic field of B=685.4 G. We phase locked the beat signal of two ECDL to the corresponding energy difference of both states. For an ideal transition the influence of scattering rates has to be minimized, while maintaining a high frequency, which leads to an optimal laser frequency between the D_1 and D_2 line. A Rabi frequency of $\Omega_R = 2\pi \times (130.7 \pm 0.2)$ kHz was achieved.

Zusammenfassung

Diese Arbeit präsentiert das Treiben von Ramanübergängen zwischen zwei hyperfeinen Grundzuständen in ultrakalten ^{6}Li Atomen mithilfe einer optischen Phasenregelschleife. Ramanübergänge bieten eine Möglichkeit für schnellen Populationstransfer mit hoher räumlicher Auflösung zur Aufhebung von Wechselwirkungen, z.B. zur Messung der Impulsverteilung einer expandierenden Atomwolke. Die entscheidende Bedingung hierbei ist die Kohärenz beider Lichtfelder, relatives Phasenrauschen würde den Übergang unterdrücken. Um eine Phasenstabilität während des Experiments zu gewährleisten wurde eine optische Phasenregelschleife verwendet, die einen der beiden verwendeten Laser kontinuierlich reguliert, sodass eine stabile Phasen- und Frequenzbeziehung zum zweiten Laser besteht. Es wurden Ramanübergänge zwischen den Grundzuständen $|3\rangle$ und $|4\rangle$ bei einem magnetischen Feld von B=685.4 G getrieben. Dazu wurde das Beat Signal zweier ECDL bei einer Frequenz, die dem Energieunterschied der Zustände entspricht, phasenstabilisiert. Für einen idealen Übergang muss der Einfluss der Streurate, unter Beibehalten einer hohen Frequenz, minimiert werden, was eine optimale Laserfrequenz zwischen der D_1 und D_2 Linie zur Folge hat. Es wurde eine Rabifrequenz von $\Omega_R = 2\pi \times (130.7 \pm 0.2)$ kHz erreicht.

Contents

1 Introduction

In order to investigate the quantum mechanical behaviour of Fermions our group performs experiments with ultracold ^{6}Li atoms. Through various cooling techniques temperatures in the nK region can be reached [1]. The experiments are performed with two of the lowest three Zeeman sublevels at a magnetic field between 300 and 1200 G. Figure 1.1 (a) shows the magnetic field dependence of the ground state.

An exciting regime is the so called unitary regime in which the gas is still dilute but the scattering length diverges, hence all length scales of the system disappear and the system exhibits universal behaviour. However, in order to probe such systems in ultracold gases typically a time-of-flight method is used in which the atoms expand and are then imaged. During the expansion though, the atoms should be non-interacting in order to preserve the initial quantum state. To avoid this interaction one of the two states has to be transferred to one of the highest three Zeeman sublevels. The energy difference corresponds roughly to a frequency of 1 GHz, therefore a direct transition requires microwave radiation, which results in a poor spatial resolution and makes quick transitions hard, since the beams intensities are not sufficient [2].

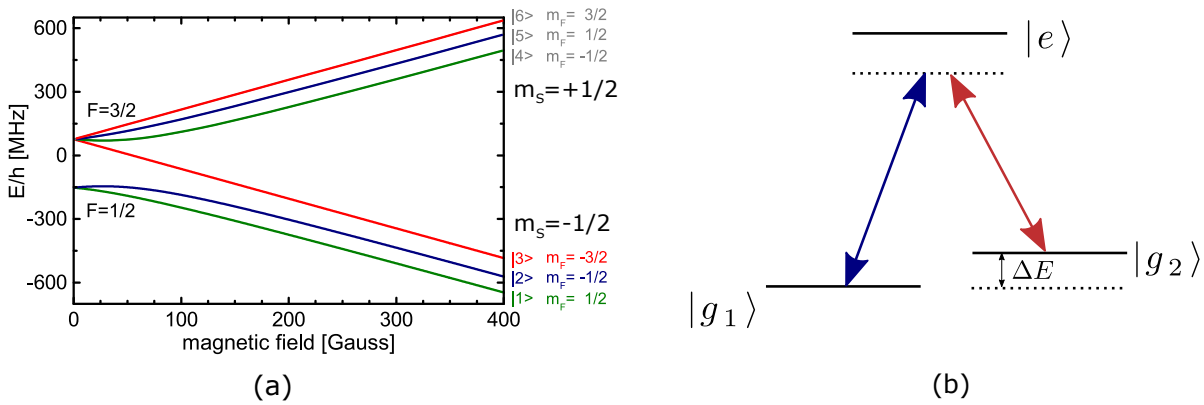

Figure 1.1: (a) Zeeman splitting of the gorund state of ^{6}Li. Taken and adapted from [3] (b) Basic scheme of a Raman transitions between two ground states $|g_1\rangle$ and $|g_2\rangle$

A high Rabi frequency for quick population transfer can be achieved by a Raman transition. Both ground states $|g_1\rangle$ and $|g_2\rangle$ are coupled by two laser beams, with frequency difference corresponding to the energy difference, via an exited state $|e\rangle$. Actual excitation to $|e\rangle$ can be avoided by detuning both beams from the resonant transition. Hence

$|e\rangle$ is effectively not populated and we have population transfer between $|g_1\rangle$ and $|g_2\rangle$.

To properly drive a Raman transition the system has to be in a coherent superposition of states $|g_1\rangle, |g_2\rangle$ and $|e\rangle$, which implies a high level of phase stability between both beams. Relative phase noise would introduce decoherence and suppress the transition. Raman transitions between state $|1\rangle$ and $|2\rangle$ were already successfully performed in our group [4]. There only one laser was used and both beams were created by splitting the initial beam and sending one part through an AOM, which shifted the frequency by 80 MHz, hence both beams had the frequency difference needed. Phase coherence is automatically guaranteed by this method, since only one laser is used.

Unfortunately this method can not be used for driving a transition between one of the lowest three Zeeman levels to $|4\rangle, |5\rangle$ or $|6\rangle$ as their frequency difference is around 2 GHz for high fields, too high for an AOM. We therefore have to use another method. One possible way would be to use two different lasers with the corresponding frequency difference. To ensure phase stability between both lasers an optical phase locked loop (OPLL) can be employed [2]. The OPLL regulates one laser such that a stable phase and frequency difference to the other laser is maintained over time. Thus relative phase noise is reduced to a minimum and coherence between both beams is provided.

Outline

In the first two sections the fundamentals of Raman transitions and Phase locked loops are introduced. Section 4 gives a brief overview of cooling and trapping Lithium and presents the phase lock setup used in our experiment. The measurements of Raman transitions, beat signals stabilized by the OPLL and spectra of one laser used in the experiment are shown in section 5 and finally a conclusion and outlook is given in section 6.

2 Raman Transitions

2.1 Basic Theory

In this section we want to set out the basic theoretical concepts that are necessary to describe Raman transitions in an atom.
The atom is reduced to a three level system in which the lower two states are ground states, while the upper one represents an excited state. Coupling state $|1\rangle$ with the pump laser to state $|3\rangle$, whereas the stokes laser couples $|2\rangle$ and $|3\rangle$ results in a Λ-configuration as shown in figure 2.1.

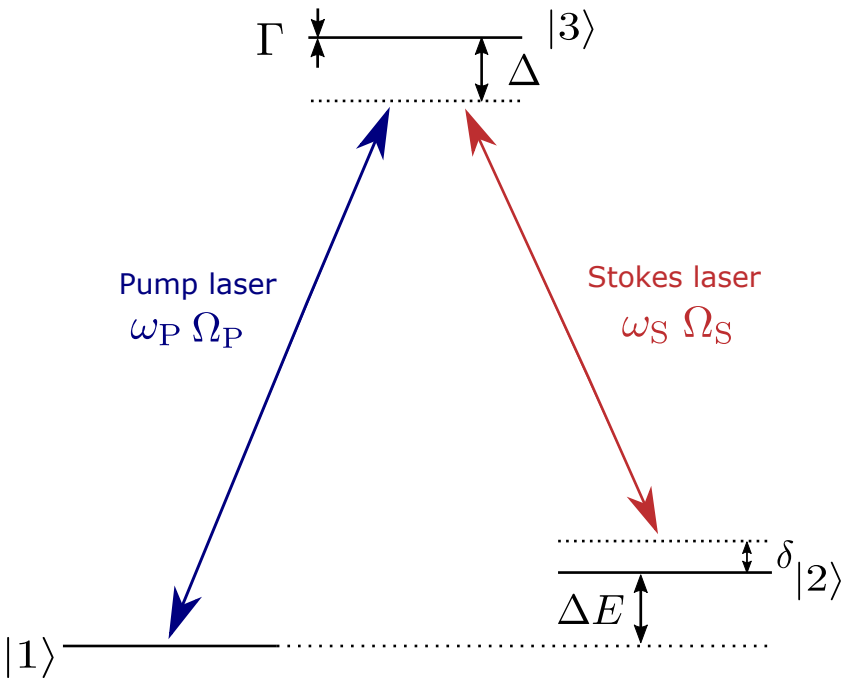

Figure 2.1: Raman transition in a Λ configuration. Two ground states $|1\rangle$ and $|2\rangle$ are coupled via $|3\rangle$ by Stokes and Pump laser. A large detuning Δ avoids excitation in $|3\rangle$.

A Raman transition is a coherent population transfer between states $|1\rangle$ and $|2\rangle$. Simultaneous to being in an intermediate virtual state through absorption of a photon from the pump laser the system undergoes a transition to $|2\rangle$ by stimulated emission of a photon from the Stokes laser. This coherent two-photon process requires the detuning

Δ of each laser beam from the intermediate state to be much larger than the linewidth Γ, to avoid excitation in $|3\rangle$. Hence $|3\rangle$ is not effectively populated. Since the transfer occurs in the same way from $|2\rangle$ to $|1\rangle$, this results in an oscillating population of the two lower states with Rabi frequency Ω_R.

If not mentioned otherwise the following derivation is adapted from [5]. In order to derive the Rabi frequency we apply a quantum mechanical treatment to the system, i. e. we solve the Schrödinger equation.

$$i\hbar\frac{\partial}{\partial t}|\Psi(t)\rangle = \hat{H}|\Psi(t)\rangle \tag{2.1}$$

The atom-light interaction is treated as a perturbation $\hat{H}_{int}$ of the isolated atom $\hat{H}_0$. The full Hamiltonian is $\hat{H} = \hat{H}_0 + \hat{H}_{int}$ with

$$\hat{H}_{int} = -\hat{\mathbf{d}}\cdot\mathbf{E} = -\hat{\mathbf{d}}\cdot(\mathbf{E}_P + \mathbf{E}_S) \tag{2.2}$$

where $-\hat{\mathbf{d}}$ is the dipole moment operator of the atom and

$$\begin{aligned}\mathbf{E}_P &= \mathbf{E}_{P_0}\exp(-i\omega_P t)\\ \mathbf{E}_S &= \mathbf{E}_{S_0}\exp(-i\omega_S t)\end{aligned} \tag{2.3}$$

are the light fields of the lasers.
Writing $|\Psi(t)\rangle$ as a superposition of the basis states

$$|\Psi(t)\rangle = c_1(t)|1\rangle + c_2(t)|2\rangle + c_3(t)|3\rangle \tag{2.4}$$

the Schrödinger equation becomes

$$i\hbar\frac{\partial}{\partial t}\mathbf{c}(t) = \hat{H}\mathbf{c}(t) \tag{2.5}$$

with $\mathbf{c}(t) = [c_1(t), c_2(t), c_3(t)]^T$. The probability to measure the system in state $|i\rangle$ is $|c_i(t)|^2$. Using the rotating wave approximation (RWA) the Hamiltonian in the ordered basis $\{|1\rangle, |2\rangle, |3\rangle\}$ can be written:

$$\hat{H} = \frac{\hbar}{2}\begin{pmatrix} 0 & 0 & \Omega_P \\ 0 & -2\delta & \Omega_S \\ \Omega_P & \Omega_S & -2\Delta \end{pmatrix} \tag{2.6}$$

Where δ is the detuning from two photon resonance and Ω_i are the Rabi frequencies of the individual transitions.

$$\begin{aligned}\Omega_p &= \frac{\langle 2|\,\mathbf{d}\cdot\mathbf{E}_{P_0}\,|3\rangle}{\hbar}\\ \Omega_s &= \frac{\langle 1|\,\mathbf{d}\cdot\mathbf{E}_{S_0}\,|2\rangle}{\hbar}\end{aligned} \tag{2.7}$$

The individual Rabi frequency can be written in terms of the beam intensity I

$$\Omega = \Gamma\sqrt{\frac{I}{I_0}} \tag{2.8}$$

where Γ is the linewidth of the exited level and I_0 the saturation intensity.

Plugging (2.6) into (2.5) yields a set of linear differential equations for the probability amplitudes:

$$\begin{aligned} i\frac{\partial c_1}{\partial t} &= \frac{1}{2}\Omega_{pP}c_3 \\ i\frac{\partial c_2}{\partial t} &= \frac{1}{2}\Omega_S c_3 - \delta c_2 \\ i\frac{\partial c_3}{\partial t} &= \frac{1}{2}(\Omega_P c_1 + \Omega_S c_2) - \Delta c_3 \end{aligned} \tag{2.9}$$

Now we want to apply adiabatic elimination which is a basic tool for reduction of complex quantum systems by removing the weakly coupled states. As population of $|3\rangle$ is strongly suppressed adiabatic elimination can be achieved by setting $\partial_t c_3 = 0$, leaving us with an effective two level system:

$$\begin{aligned} i\frac{\partial c_1}{\partial t} &= \frac{\Omega_P}{4\Delta}(\Omega_P c_1 + \Omega_S c_2) \\ i\frac{\partial c_2}{\partial t} &= \frac{\Omega_S}{4\Delta}(\Omega_P c_1 + \Omega_S c_2) - \delta c_2 \end{aligned} \tag{2.10}$$

With Hamiltonian:

$$\hat{H}_{eff} = \frac{\hbar}{2}\begin{pmatrix} \frac{\Omega_P^2}{2\Delta} & \frac{\Omega_P\Omega_S}{2\Delta} \\ \frac{\Omega_P\Omega_S}{2\Delta} & \frac{\Omega_S^2}{2\Delta} - 2\delta \end{pmatrix} \tag{2.11}$$

Just like in a two level system the off diagonal elements describe the coupling of states $|1\rangle$ and $|2\rangle$ via both laser beams. Solving the equations with the atom being initially in state $|1\rangle$ yields the time evolution of the population:

$$\begin{aligned} |c_1(t)|^2 &= 1 - \frac{\Omega_R^2}{\Omega_0^2}\sin^2\left(\frac{\Omega_0 t}{2}\right) \\ |c_2(t)|^2 &= \frac{\Omega_R^2}{\Omega_0^2}\sin^2\left(\frac{\Omega_0 t}{2}\right) \end{aligned} \tag{2.12}$$

Where

$$\Omega_R = \frac{\Omega_P\Omega_S}{2\Delta} \tag{2.13}$$

is the Rabi frequancy of the resonant transition ($\delta = 0$) and $\Omega_0 = \sqrt{\Omega_R^2 + \delta^2}$ is the effective Rabi frequency.

Note that a coherent Raman transition involving simultaneous absorption and stimulated emission is fundamentally different from two successive single photon processes. But even

with a detuning from the resonance frequency the atom can be excited. The scattering rate of a laser beam with detuning Δ is given by [6]

$$\Gamma_{\mathrm{sc}} = \frac{\Gamma}{2} \frac{\Omega^2/2}{\Delta^2 + \Omega^2/2 + \Gamma^2/4} \tag{2.14}$$

Where Γ is the linewidth and Ω the Rabi frequency. With large detuning $\Delta \gg \Gamma$ and since $\Delta \gg \Omega$ this becomes approximately

$$\Gamma_{\mathrm{sc}} \simeq \frac{\Gamma\Omega^2}{4\Delta^2} \tag{2.15}$$

Consider a π-pulse containing both laser frequencies ω_p and ω_s with duration t_π:

$$\Omega_0 t_\pi = \pi \tag{2.16}$$

Note that this means a complete period for oscillation of the population $|c_i|^2$, whereas the components c_i oscillate with half the frequency $\Omega_0/2$, sometimes the latter is referred to as Rabi frequency. Assuming that both beams have similar intensities such that $\Omega_p \simeq \Omega_s \equiv \Omega$ and therefore $\Omega_0 \simeq \Omega^2/2\Delta$. The number of spontaneously emitted photons during the pulse is then [6]

$$\Gamma_{\mathrm{sc}} t_\pi \simeq \frac{\pi\Gamma}{2\Delta} \tag{2.17}$$

Hence spontaneous emission can be neglected if the detuning is sufficiently large resulting in $R_{scatt} t_\pi \ll 1$ and the atom can be subjected to many π-pulses before a spontaneous emission occurs and destroys the coherence.

The Rabi frequency however also decreases with lager detuning. Furthermore we only discussed three-level systems so far. Unfortunately life is not that simple. In reality there are several more exited states that must be taken into account and lager detuning does not necessarily lead to better Rabi oscillations. We have two main gaols, we want a high ratio between Rabi frequency Ω_R and single photon scattering event, called β factor

$$\beta = \frac{\Omega_R}{\Gamma_{scatt}} \tag{2.18}$$

and a high Rabi frequency.

2.2 Raman Transitions in Lithium

2.2.1 Properties of ^{6}Li

We will drive Raman transitions on ultra-cold ^{6}Li atoms. So let's get familiar with some basic properties of Lithium. The information presented here is taken from the standard reference for Lithium [7], where further details can be found. The ground state of ^{6}Li has

the configuration $1s^2 2s^1$. It has a single valence electron, which makes it an alkali metal and therefore similar to hydrogen. The advantage of this are a simple level structure and easier calculations. ^{6}Li is the lightest of alkali metals, which makes tunneling rates higher than for other alkalis, as they decrease with mass. Raman transitions however turn out to be rather challenging with Lithium since β - factors of other alkalis are higher by a factor of $\sim 10^3$ [8]. This is due to the low fine and hyperfine splitting in Lithium compared to other alkalis. For instance Rubidium has a fine structure splitting of ~ 15 nm between D_1 and D_2 line [9]. We are therefore limited by orders of magnitude higher scattering rates in Lithium.

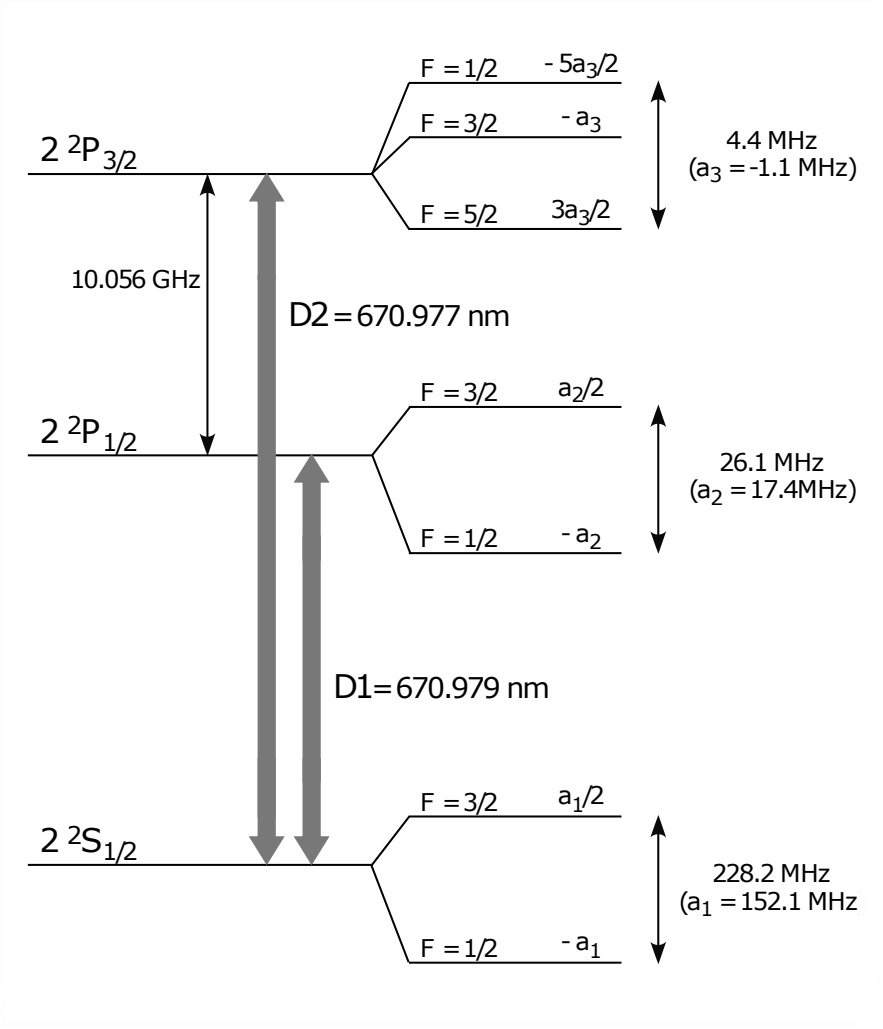

Figure 2.2: Energy level diagram of ^{6}Li with fine and hyperfine splitting. Taken from [7].

In figure 2.2 one can see the energy level diagram of ^{6}Li, the transition from excited state 2^2P to the ground state 2^2S (the D-line) splits into two transitions. This is the

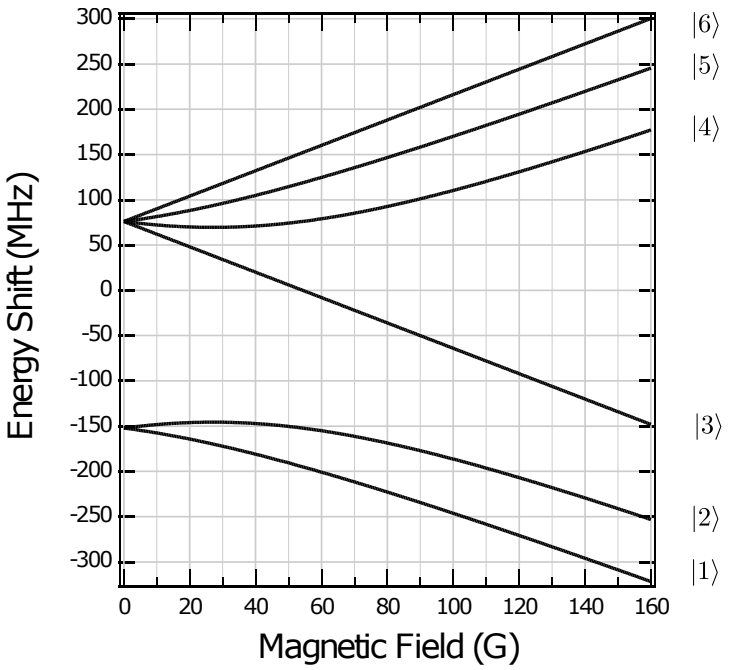

Figure 2.3: Magnetic field dependence of the ground state $2^2P_{1/2}$. Taken and adapted from [7].

fine structure splitting, the cause of which is the coupling of orbital angular momentum $\mathbf{L}$ with the spin $\mathbf{S}$. These add vectorially to the angular momentum $\mathbf{J} = \mathbf{L} + \mathbf{S}$. The quantum number J can take values in integer steps between

$$|L - S| \leq J \leq (L + S) \tag{2.19}$$

Thus the D line is split into transitions $2^2P_{3/2} \longleftrightarrow 2^2S_{1/2}$ (D_2) and $2^2P_{1/2} \longleftrightarrow 2^2S_{1/2}$($D_1$). With energy difference of both lines around $2\pi \times 10$ GHz. The last splitting in absence of an external magnetic field is due to the interaction between nuclear spin $\mathbf{I}$ and $\mathbf{J}$. This is described by the total atomic angular momentum $\mathbf{F} = \mathbf{J} + \mathbf{I}$. F can take values in integer steps between

$$|J - I| \leq F \leq (J + I) \tag{2.20}$$

^{6}Li has nuclear spin $I = 1$, therefore $2^2S_{1/2}$ and $2^2P_{1/2}$ split into two lines, while $2^2P_{3/2}$ splits into three. The energy shift due to hyperfine is roughly a factor of 10^3 smaller than fine structure splitting. Note that the energy diagram in figure 2.2 is not to scale.

When applying an external magnetic field the hyperfine levels are split into $2F + 1$ sublevel. For small fields we are in the linear Zeeman regime, the energy is split linear with magnetic field B

$$\Delta E = \frac{\mu_B}{\hbar} g_F m_F B \tag{2.21}$$

where μ_B is the Bohr magneton and g_F the Lande factor. For higher fields nuclear spin starts to decouple from angular momentum, and we are no longer in the linear Zeeman

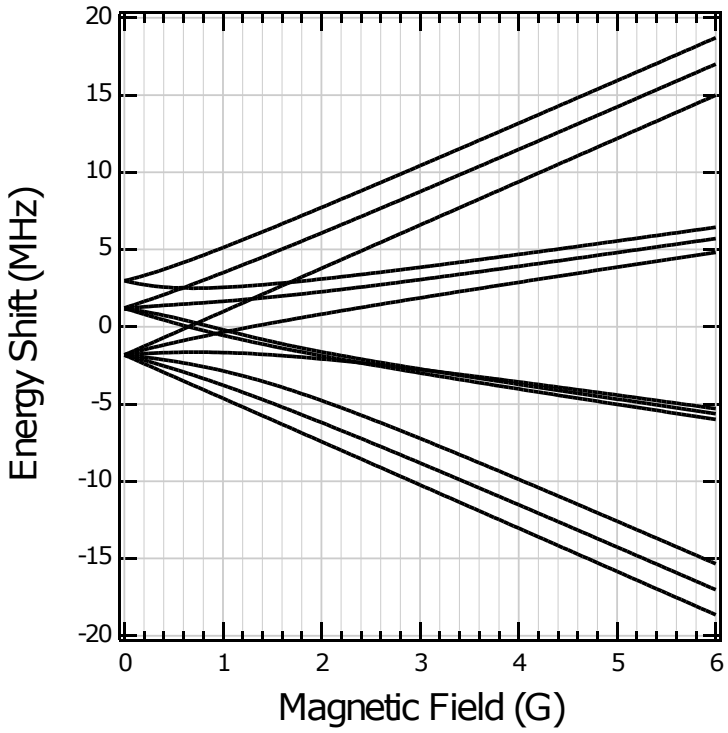

Figure 2.4: Magnetic field dependence of the exited state $2^2P_{3/2}$. Taken from [7].

regime. This can be seen in figure 2.3 and 2.4. The decoupling already happens for 10-20 G for the ground state and 1 G for the exited $2^2P_{3/2}$ state, which causes the energy lines to bend. If the magnetic field is now increased further nuclear spin and angular momentum are completely decoupled. The states are now labeled with numbers, starting from the lowest energy state as can be seen in figure 2.3. The ground states $|3\rangle$ and $|4\rangle$ are our candidates for Raman transitions.

2.2.2 Multilevel Raman Transitions

As mentioned earlier, there are several excited states that need to be considered. The D_1 line splits into 6 and the D_2 into 12 sublevels. The equations (2.12) for populations still remain valid. However, we need to be more precise when calculating the Rabi frequency and scattering rate. Not all 18 excited states are available to drive a Raman transition, because due to polarization of the beams not all states are coupled to the ground states, for certain pairs of polarization even no Raman transition is possible, but more than one excited state remains to be considered.

Raman transitions in alkali metals exposed to an external magnetic field are discussed in [8], on which we have based our calculations and where further information can be found. We will summarize the main results here.
We consider two ground states $|g_1\rangle$ and $|g_2\rangle$ coupled to a pair of exited multiplets $\{|e_\mu\rangle, |e_\nu\rangle\}$ by two laser beams. The states $|e_\mu\rangle$ and $|e_\mu\rangle$ are states in the J=1/2 (D_1)

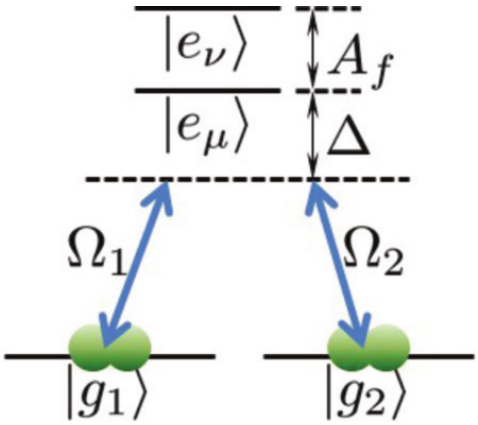

Figure 2.5: Multilevel Raman transition. Both ground states are coupled to exited states e_μ and e_ν from the D_1 and D_2 line by two lasers with detuning Δ from the D_1 line. Taken from [8].

and J=3/2 (D_2) manifolds with energies E_μ and E_ν. For ^{6}Li the energy difference $A_f = E_\nu - E_\mu$ is around $2\pi \times 10$ GHz. Let Δ be the energy mismatch between laser frequency and the D_1 transition. The Rabi frequency then becomes

$$\Omega_R = \sum_\mu \frac{\Omega_{1\mu}\Omega_{2\mu}}{2\Delta} + \sum_\nu \frac{\Omega_{1\nu}\Omega_{2\nu}}{2(\Delta + A_f)} \tag{2.22}$$

where $\Omega_{i\epsilon} = \mathbf{E}_i \cdot \langle g_i | \mathbf{d} | e_\epsilon \rangle / \hbar$ is the optical Rabi frequency of each individual transition. In the first sum we add up all states from the D_1 line coupled to the ground states by both lasers and the second sum adds up all states from the D_2 line, therefore the detuning is increased by A_f. The ground state quadrupole matrix element $\langle g_1 | d_a d_b | g_j \rangle = 0$, unless $i = j$ and $a = b$ $(a, b = x, y, z)$. This is due to the spherical symmetry of the electron wave function and the fact that electronic dipole does not couple to spin. We then find $\sum_\mu \Omega_{1\mu}\Omega_{2\mu} + \sum_\nu \Omega_{1\nu}\Omega_{2\nu} = 0$ and can simplify the equation above to

$$\Omega_R = \frac{A_f}{2\Delta(\Delta + A_f)} \sum_\mu \Omega_{1\mu}\Omega_{2\mu} \tag{2.23}$$

which for a big detuning $\Delta \gg A_f$ can be approximated to $\Omega_R \sim A_f/\Delta^2$. This however does not apply to our case, since we will detune our lasers red to the D_2 and blue to the D_1 line.

The inelastic scattering rate emerging from spontaneous emission of the exited states is given by

$$\Gamma_{\mathrm{sc}} = \gamma \left[\sum_\mu \frac{(\Omega_{1\mu}^2 + \Omega_{2\mu}^2)}{4\Delta^2} + \sum_\nu \frac{(\Omega_{1\nu}^2 + \Omega_{2\nu}^2)}{4(\Delta + A_f)^2} \right] \tag{2.24}$$

To calculate the Rabi frequency and scattering rate one needs to calculate $\Omega_{i\epsilon}$ and its dependence on the magnetic field, therefore we have to diagonalize the Hamiltonian. The fine and hyperfine structure of an alkali metal is described by a coupled spin Hamiltonian

$$H = H_a + H_B \tag{2.25}$$

with

$$H_a = c_f \mathbf{L}\cdot\mathbf{S} + c_{hf1}\mathbf{L}\cdot\mathbf{I} + c_{hf2}\mathbf{S}\cdot\mathbf{I} \tag{2.26}$$
$$H_B = \mu_B(g_L\mathbf{L} + g_S\mathbf{S} + g_I\mathbf{I})\cdot\mathbf{B} \tag{2.27}$$

This Hamiltonian can now be diagonalized in the basis $|Lm_Lm_Sm_I\rangle$ and the eigenstate $|LQ\rangle$ can be expanded

$$|LQ\rangle = \sum_{m_Lm_Sm_I} C^Q_{m_Lm_Sm_I}\,|Lm_Lm_Sm_I\rangle \tag{2.28}$$

with coefficients $C^Q_{m_Lm_Sm_I}$, which will be used to calculate the electronic dipole transition. Let $D_q = \langle Lm_Lm_Sm_I|\, er_q\,|L'm'_Lm'_Sm'_I\rangle$ be the electronic dipole transition between state $|L'm'_Lm'_Sm'_I\rangle$ and $|Lm_Lm_Sm_I\rangle$, where r_q is a spherical tensor and $q = -1, 0, +1$ corresponds to σ^-, π and σ^+ polarized light. The electric dipole does not directly couple electron or nuclear spin and the dipole transition can be written $D_q = \delta_{m_Sm'_S}\delta_{m_Im'_I}\langle Lm_L|\, er_q\,|L'm'_L\rangle$. Using the Wigner-Eckart theorem we can further simplify this to $D_q = \delta_{m_Sm'_S}\delta_{m_Im'_I}W^{L'L}_{m'_Lqm_L}\langle L|\,|er_q|\,|L'\rangle$. Where $W^{L'L}_{m'_Lqm_L}$ can be written in with a Wigner 3-j symbol

$$W^{L'L}_{m'_Lqm_L} = (-1)^{L'-1+m_L}\sqrt{2L+1}\begin{pmatrix} L' & 1 & L \\ m'_L & q & -m_l\end{pmatrix} \tag{2.29}$$

The electronic dipole transition $D^{L'Q'}_{q,LQ}$ between two states $|LQ\rangle$ and $|L'Q'\rangle$ can then finally be written

$$D^{L'Q'}_{q,LQ} \equiv \langle LQ|\, er_q\,|L'Q'\rangle \tag{2.30}$$
$$= \sum_{\bar m_L\bar m'_L\bar m_S\bar m_I} C^Q_{\bar m_L\bar m_S\bar m_I}C_{\bar m'_L\bar m_S\bar m_I}W^{L'L}_{m'_Lqm_L}\langle L|\,|er_q|\,|L'\rangle \tag{2.31}$$

This was all done and implemented in Python by Laurin Fischer from our group, which we used for our theoretical calculation of electric dipole transitions, Rabi frequencies and β factors.

3 Phase Locked Loops

Phase-locked loops (PLL) are widely used in radio-frequency engineering, computers and other applications. The basic idea is to stabilize phase and frequency of an oscillator to a reference signal. By continuously keeping track of the phase error between reference and oscillator, small adjustments to the tuning voltage of the oscillator are made by the PLL in order to regulate its phase and thus providing a stable signal. The optical-phase-locked loop (OPLL), which will be used in our experiment is a special PLL, stabilising the beat signal of two laser beams.

3.1 Basics of Control Theory

In order to analyse the PLL and its components in detail, we must first introduce a few concepts of Control Theory. We call the components in our loop systems. A system transforms a time dependent input signal $x(t)$ to an output signal $y(t)$.

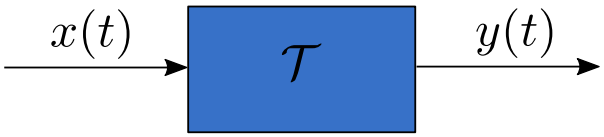

Figure 3.1: Typical visualisation of a system generating the output $y(t) = \mathcal{T}\{x(t)\}$

From a mathematical point of view, a system is a self mapping operator $\mathcal{T}$ on the set of time dependent functions.
Control theory deals with linear time-invariant (LTI) systems, using the Laplace transform as a key tool for analysis. So let's define these terms first.

LTI-Systems
A system is *linear* if the sum of any number of input signals $x_i(t)$ transforms proportional to the sum of their output signals $y_i(t)$.

$$\mathcal{T}\left\{\sum_i \lambda_i x_i(t)\right\} = \sum_i \lambda_i \mathcal{T}\{x_i(t)\} = \sum_i \lambda_i y_i(t) \tag{3.1}$$

A system is *time independent* if it reacts to a time delayed input by the same output except for the time delay.

$$\mathcal{T}\{x(t-t_0)\} = y(t-t_0) \tag{3.2}$$

Laplace transform
The Laplace transform maps a function of real time f to a function of complex frequency F. For a function $f : \mathbb{R}_+ \longrightarrow \mathbb{C}$ the Laplace transform $\mathcal{L} = F : \mathbb{C} \longrightarrow \mathbb{C}$ is defined by

$$\mathcal{L}\{f(t)\} = F(s) = \int_0^\infty f(t)\mathrm{e}^{-st}\,dt \tag{3.3}$$

if the integral exists. For our intentions the transform of a derivative, an integral and of a time delay are of particular interest.The transform of a derivative is

$$\mathcal{L}\left\{\frac{df}{dt}\right\} = sF(s) - f(0) \tag{3.4}$$

With initial condition $f(0) = 0$ this becomes a simple multiplication of the transform with s. Since integration is the inverse operation of differentiating one can guess that the Laplace transform of an integral corresponds to a division by s.
In fact this is exactly what we get.

$$\mathcal{L}\left\{\int_0^t f(\xi)\,d\xi\right\} = \frac{1}{s}F(s) \tag{3.5}$$

Signals are often not instantaneously transmitted. The Laplace transform of a signal delayed by τ is given by

$$\mathcal{L}\{f(t-\tau)\Theta(t-\tau)\} = F(s)\mathrm{e}^{-s\tau} \tag{3.6}$$

where Θ is the unit step function. For continuous LTI systems the **transfer function** $H(s)$ describes the relation between an input $x(t)$ and an output signal $y(t)$ in the Laplace domain. It is defined as

$$H(s) = \frac{Y(s)}{X(s)} = \frac{\mathcal{L}\{y(t)\}}{\mathcal{L}\{x(t)\}} \tag{3.7}$$

It is common to use capital letters for Laplace transformed quantities. One can also read the above equations as $Y(s) = H(s)X(s)$, thus the transfer function is a linear mapping of the transformed input to the transformed output. Consider a system creating its output by integrating the input $y(t) = \int_0^t x(\xi)\,d\xi$. Because of (3.5) the transfer function then is given by $H(s) = 1/s$.
The advantage of describing systems in the Laplace domain becomes apparent when we consider a composition of two systems. The overall transfer function is simply the product of each individual transfer function $H(s) = H_1(s)H_2(s)$.

3.2 Analysis of PLLs

A PLL is a feedback control system, mainly consisting of two oscillators (reference and slave), a Phase-Frequency detector (PFD) and a Loop Filter. A basic scheme can be seen in Figure 3. The goal is to stabilize the signal of our slave oscillator, also called voltage

controlled oscillator (VCO), since its frequency is determined by the tuning voltage, to the reference and thus not only ensuring a stable frequency but also a fixed phase of the VCO.

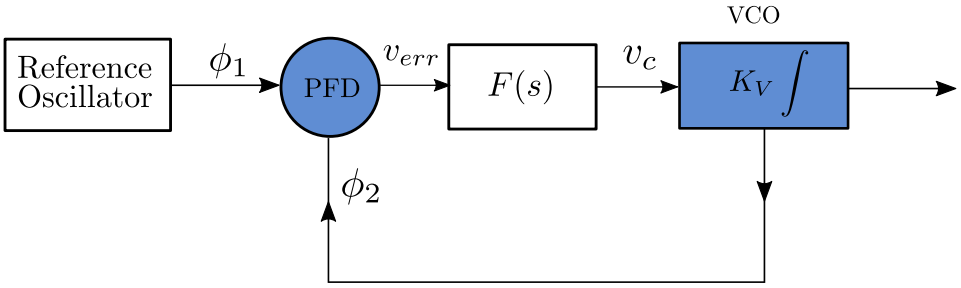

Figure 3.2: By comparing reference and VCO signal the PFD produces an error signal, wich after futher processing by the Loop Filter is fed back in to VCO

Although the components in general show nonlinear behaviour its justified to assume linearity if dealing only with small variations, i.e. $\phi_r(t) \approx \phi_0(t)$ and the methods introduced above can be applied. Before being fed into the PFD the signals are usually divided down $\phi_r(t) = \frac{1}{R}\phi_{ref}$ and $\phi_0(t) = \frac{1}{N}\phi_{VCO}$. The PFD then generates an error signal proportional to the phase difference $v_{err}(t) = K_d(\phi_r(t) - \phi_0(t))$ with proportionality constant K_d or in the Laplace domain

$$V_{err}(s) = K_d(\Phi_r(s) - \Phi_0(s)) \tag{3.8}$$

One important task of the Loop Filter is to integrate and filter the error signal from the VCO. Key entities concerning stability of the loop like bandwidth and phase are mainly determined by the Loop Filter with transfer function $F(s)$. The VCO reacts to a change of its tuning voltage v_c with a proportional shift in its frequency $\Delta\omega$ and since frequency is the derivative of phase we get:

$$\frac{d\phi_{VCO}}{dt} = \Delta\omega(t) = K_V v_c(t) \tag{3.9}$$

Since the incoming signal is integrated by the VCO this results in a change of phase $\phi_{VCO}(t) = K_V \int_0^t v_c(\xi)\, d\xi$. With (3.5) the relation in the Laplace domain becomes:

$$\Phi_{VCO}(s) = \frac{K_V V_c(s)}{s} \tag{3.10}$$

However the VCO used in our experiment is a diode laser and deviates from this ideal integrating behaviour. When modulating the laser thermal effects also have to be taken into account, which results in [2]

$$\Phi_{VCO}(s) = \frac{K_V V_c(s)}{s} \frac{1}{1 + \tau_L s} \tag{3.11}$$

where τ_L is a time constant. Another issue that has to be taken into account are delay times in the loop, since signals need time to travel.
The overall transfer function $G(s)$ (also called open loop gain) relating the down divided phase of the VCO $\Phi_0(s)$ with the phase error $\Theta(s) = \Phi_r(s) - \Phi_0(s)$ then becomes:

$$G(s) = \frac{\Phi_0(s)}{\Theta(s)} = \frac{K_d K_V F(s)}{Ns} \mathrm{e}^{-s\tau} \frac{1}{1 + \tau_L s} \tag{3.12}$$

The closed loop gain $H(s)$ relates the reference to VCO phase.

$$H(s) = \frac{\Phi_0(s)}{\Phi_r} = \frac{G(s)}{1 + G(s)} \tag{3.13}$$

The loop bandwidth is defined as frequency s_{lb} of unity gain $|G(s_{\mathrm{lb}})| = 1$.

3.2.1 Phase-frequency-detector

Digital phase detectors such as the EXOR gate, the JK-flipflop and PFD became increasingly popular as PLLs went digital. The digital PFD is the most widely used type of phase detector. As the name suggests, it can detect not only phase but also frequency differences, allowing the PLL to get locked even for large frequency offsets between the two input signals u_1 and u_2 [10].
There are basically two different designs of the PFD, a distinction is made between a voltage and a current output ("charge pump"). The PFD with voltage output has the problem of so-called backlash, this phenomenon leads to unwanted spurious frequencies ("spurs"), which can be avoided by using the charge pump design. The latter is therefore the preferred one in most applications [10].

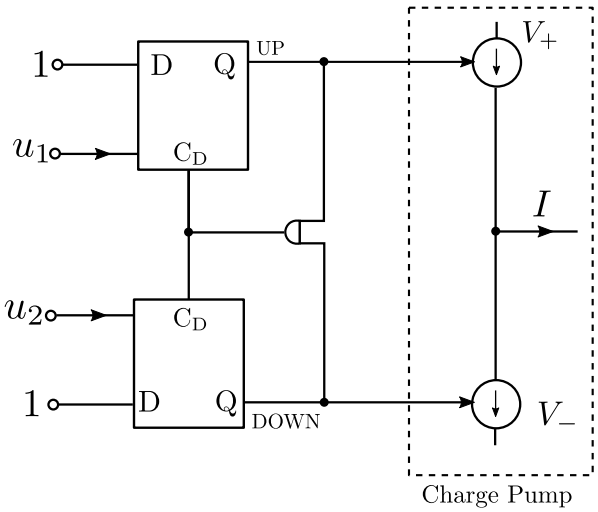

Figure 3.3: Block diagram of a PFD with current output

Figure 3.3 shows the block diagram of such a PFD. This is made up of two D flip-flops, labelled UP and DOWN and which can each take the value 0 or 1. The PFD state is one

of the 4 possible combinations of these numbers. However the state UP=1, DOWN=1 is prevented by an additional AND gate by resetting both flip-flops to zero due to the logic "high" level at their C_D "clear direct" inputs. The remaining three possible PFD states are named -1, 0 and 1 [10]:

UP	DOWN	PFD state
0	0	0
1	0	1
0	1	-1

The actual state of the PFD, how it can change and how it gets into it at all can be understood with the fact that the D-flip-flops are positive edge triggered. Rising edges of signal u_1 can trigger the UP flip-flop, while those of u_2 trigger the DOWN one. For example, if we are in the initial state 0 and a positive edge of u_1 occurs, the state changes from 0 to 1. Further positive edges of u_1 no longer change the state. It only changes when a positive edge of u_2 appears which triggers DOWN and sets the PFD back to the 0 state. If we start in the 0 state and a positive edge of u_2 appears first, the PFD is in the -1 state. In summary, positive edges of u_1 always change the state by +1 unless the state is already +1 and positive edges of u_2 by -1 unless the state is already -1. Figure 3.4 illustrates all possible state changes for all initial states.

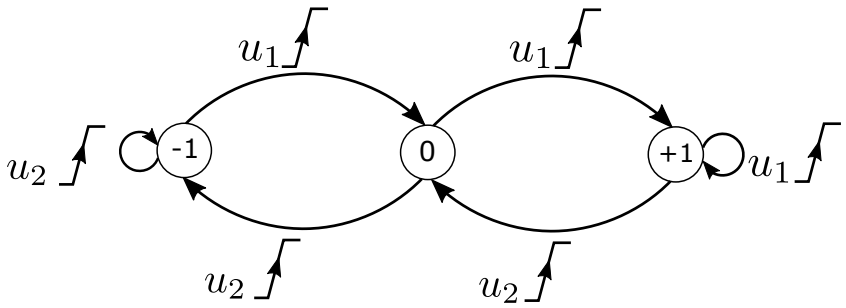

Figure 3.4: State diagram of the PFD visualising state changes due to occurring positive edges

The charge pump consists of two current sources. The upper one is active whenever the PFD is in state 1, while the lower one is active in state -1. The upper source supplies a positive current while the lower one supplies a negative one, both with the same absolute value. The total outgoing current is therefore proportional to the PFD state. Let us now look at the state and current curve for the case that two signals have the same frequency but are slightly out of phase lock. In (a) the initial state is 0 and the first positive edge is from u_1, setting the PFD state to 1 until the first positive edge from u_2 occurs. This results in positive current pulses from the charge pump, whereas in (b) the signal from u_2 leads and therefore negative current pulses leave the PFD.

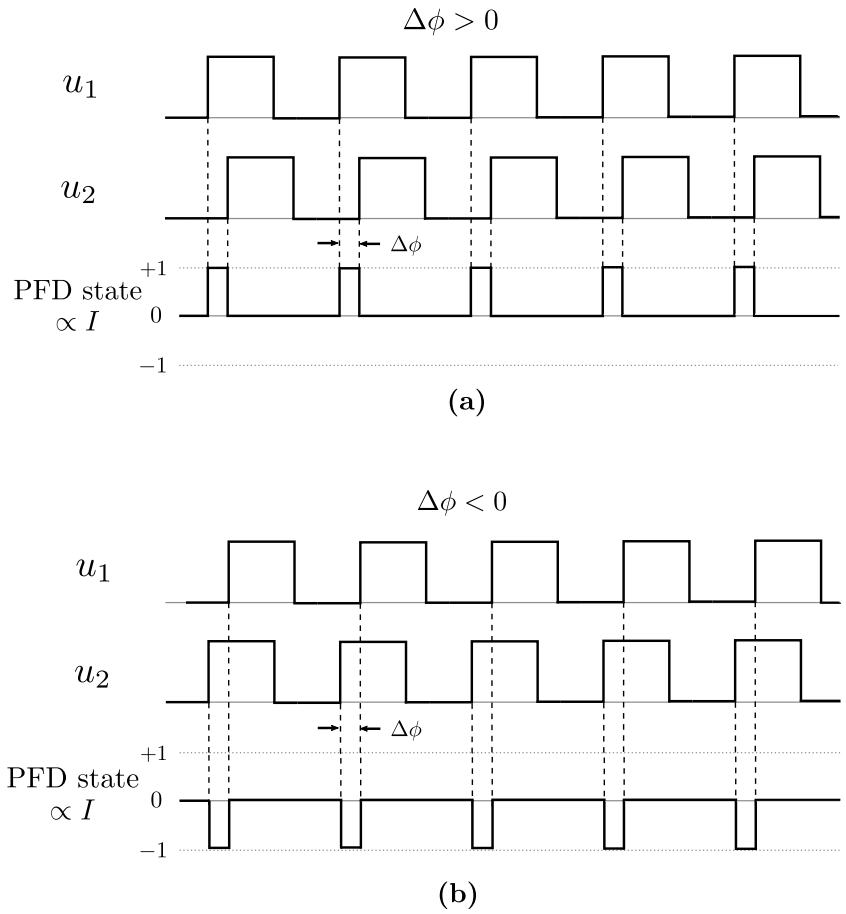

Figure 3.5: Signals u_1 and u_2 in frequency but slightly out of phase lock **(a)** positive phase error **(b)** negative phase error

The average current $\bar{I}$ is then given by

$$\begin{aligned} \bar{I} &= \frac{I_{max}}{2\pi}\Delta\phi \\ &= K_D\Delta\phi \end{aligned} \tag{3.14}$$

where I_{max} is the current amplitude and of K_D the gain factor of the PFD in (3.8). We therefore have a linear relation between $\bar{I}$ and $\Delta\phi$, which can be seen in figure 3.6. Note that the phase difference has to be understood modulo 2π.

Now one might think this is in contradiction to the equation (3.8). There, linearity of the PFD output signal to the phase difference was assumed, but the output signal for a phase difference at same frequency is a periodic current pulse. The linearity consists between mean value of the current pulses and phase difference but not between current itself and phase difference. Why can we still assume this linearity?

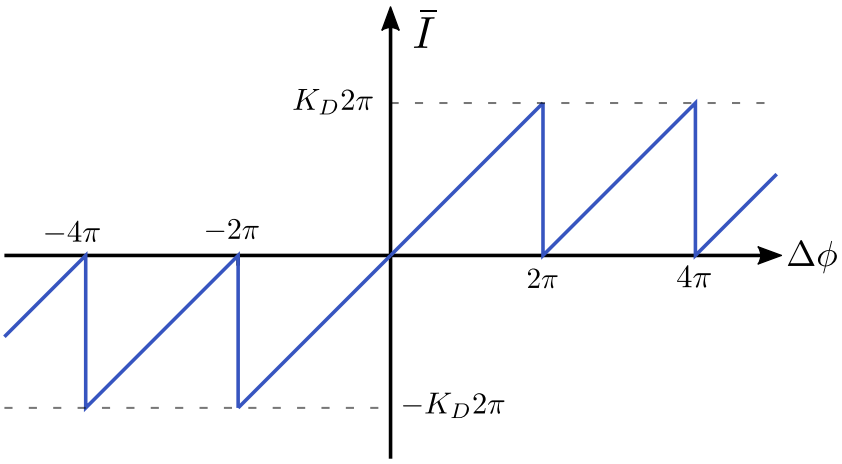

Figure 3.6: Average output current $\bar{I}$ over phase difference $\Delta\phi$

Since the output signal $I(t)$ is a periodic function, it can be expanded in a Fourier series

$$I(t) \sim \frac{a_0}{2} + \sum_{k=1}^{\infty} \left(a_k \cos(kt) + b_k \sin(kt)\right) \tag{3.15}$$

Without loss of generality we choose the period T to be 2π and our coordinate system such that $I(t)$ is a symmetric function. The antisymmetric coefficients b_k therefore vanish for all k and the remaining coefficients a_k are given by

$$a_k = \frac{1}{\pi} \int_{-\pi}^{\pi} I(t) \cos(kt)\, dt \tag{3.16}$$

Thus for $k = 0$ the integral is just twice the mean value $\bar{I}$ and we obtain $a_0/2 = \bar{I}$ as the first term of the series. Now we only have to justify, that the higher coefficients a_k for $k \geq 1$, describing the oscillating behaviour, can be neglected. The reason for this is that these higher frequencies are filtered out by the Loop Filter. This essentially determines the loop bandwidth and acts as a low-pass filter for higher frequencies than this, which also explains the general low-pass behaviour of the transfer functions G and H. The frequency of the PFD signal must be a multiple of the loop bandwidth in order to ensure a stable operation. It is recommended that the Loop bandwidth should not exceed 1/5th of the PFD frequency [2]. Filtering out high frequencies of the PFD signal is then the same as time averaging.

3.3 Optical Phase Locked Loops (OPLL)

We use an optical phase-locked loop to phase stabilize the two lasers in our experiment. Here we just want to get familiar with the basic functionality. The exact structure of the loop used in the experiment, including the characterization of each individual component, will follow later. We name the two lasers as master and slave, whereby the master laser is free-running and the slave is controlled. The two beams interfere and are sent to a photodetector. This beat signal is now stabilized to a reference. If we want to think of the OPLL as a special case of a PLL, the combination of master, slave laser and photodetector takes over the role of the VCO.

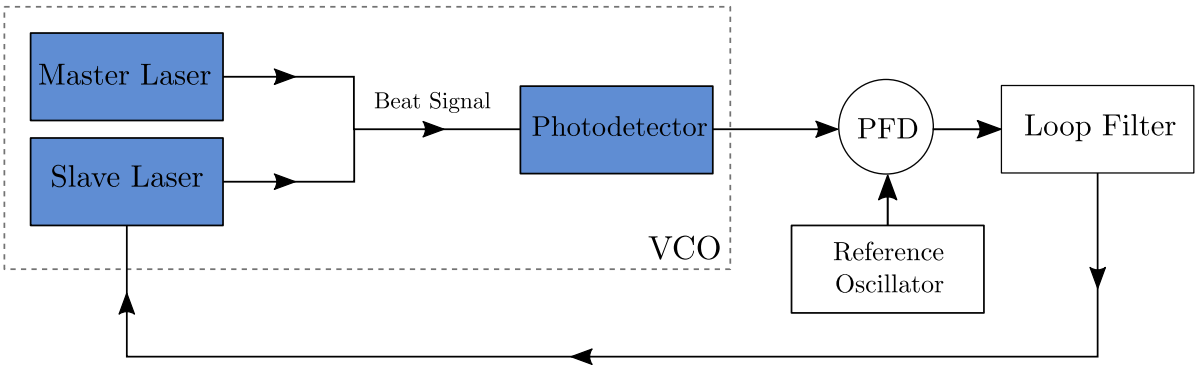

Figure 3.7: Simplified scheme of an OPLL, the Beat signal of two Laser beams is stabilised to a reference

We use a photodiode as a photodetector. Let $\mathbf{E}_i = \mathbf{E}_{i0}\cos(\omega_i t + \phi_i(t))$ be the electric fields of both laser beams, the beat signal on the photodiode has then the intensity:

$$\begin{aligned} I(t) &= \frac{1}{2} c\,\epsilon_0 \left[\mathbf{E}_1(t) + \mathbf{E}_2(t)\right]^2 \\ &= \frac{1}{2} c\,\epsilon_0 \left[\mathbf{E}_{10}\cos(\omega_1 t + \phi_1(t)) + \mathbf{E}_{20}\cos(\omega_2 t + \phi_2(t))\right]^2 \\ &= \frac{1}{2} c\,\epsilon_0 \Big[\frac{1}{2}\underbrace{\left(\mathbf{E}_1^2 + \mathbf{E}_2^2\right)}_{\text{DC}} + \underbrace{\mathbf{E}_1 \cdot \mathbf{E}_2 \cos(\Delta\omega t + \Delta\phi(t))}_{\text{slow oscillation}} \\ &\quad + \mathbf{E}_{10}^2\cos(2\omega_1 t + 2\phi_1(t)) + \mathbf{E}_{20}^2\cos(2\omega_2 t + 2\phi_2(t)) \\ &\quad + \mathbf{E}_1 \cdot \mathbf{E}_2 \cos((\omega_1 + \omega_2)t + \phi_1(t) + \phi_2(t))\Big] \end{aligned} \tag{3.17}$$

The first term is the DC part, which is filtered out by adding Bias-Tee behind the photo diode. The second term oscillates slowly with frequency $\Delta\omega = \omega_1 - \omega_2$ and phase $\Delta\phi(t) = \phi_1(t) - \phi_2(t)$. Since the bandwidth of the photo diode is usually several GHz the remaining fast oscillating terms are completely filtered out leaving us only with the slowly oscillating beat.

$$I_{\text{Beat}}(t) = \frac{1}{2} c\,\epsilon_0 \mathbf{E}_1 \cdot \mathbf{E}_2 \cos(\Delta\omega t + \Delta\phi(t)) \tag{3.18}$$

Phase stabilising the Slave to Master Laser therefore ideally means $\Delta\omega = \text{const}$ and $\Delta\phi(t) = \text{const}$.

3.3.1 External Cavity Diode Laser

For our experiments we use External Cavity Diode Lasers (ECDLs). Laser diodes offer an inexpensive, durable and compact method of generating laser light. They use recombination processes from electrons and holes at the pn-junction of a semiconductor to emit light. In case of population inversion between the valance and conduction band stimulated emission is the dominant process. Population inversion is achieved by injecting a current. The minimal current for this to happen is called threshold current I_{th}. In contrast to an individual atom we have quasi continuous energy levels in semiconductors, which lead to a broad emission spectrum of approximately $\Delta\lambda = 10$ nm. Running a laser diode single mode therefore requires additional frequency selecting elements, provided by an external cavity. In an optical cavity of length L only modes of the light can exist, which are capable of forming standing waves. This limits the allowed wavelengths to

$$k\,\frac{\lambda}{2} = L \quad k \in \mathbb{N} \tag{3.19}$$

We have two cavities in our lasers. One cavity is the laser diode itself. The amplified wavelengths are far apart and wide. The external cavity consists of a blaze grating in Littrow configuration, which reflects the first order back into the diode, while the zeroth order is decoupled and available as laser light.

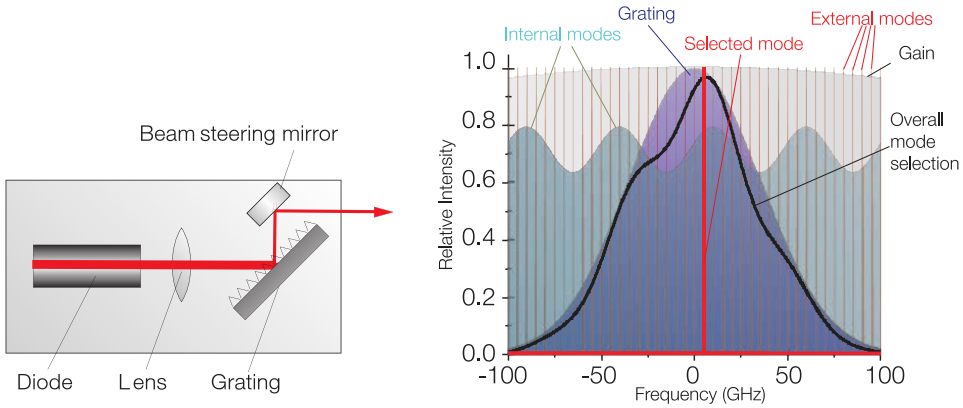

Figure 3.8: Left: Littrow configuration ECDL Right: The overall gain is formed by combination of the different gain profiles. Taken from [11]

The output power of a laser diode depends on the injection current and the temperature. Figure 3.9 shows such a curve for constant temperature. Above the threshold current I_{th} the power increases sharply, whereas below it only increases slightly. Here we are in the regime of spontaneous emission with a large spectral width, similar to an LED. The threshold current increases with temperature. After passing I_{th}, spontaneous emission with a narrow line width dominates. Electrical power is now efficiently converted into

optical power. This is commonly characterised with the differential slope efficiency, which is the slope above threshold current. Figure 3.10 shows the spectra of the Toptica DL pro used in our laboratory for both regions.

$$\eta = \frac{\Delta P}{\Delta I} \tag{3.20}$$

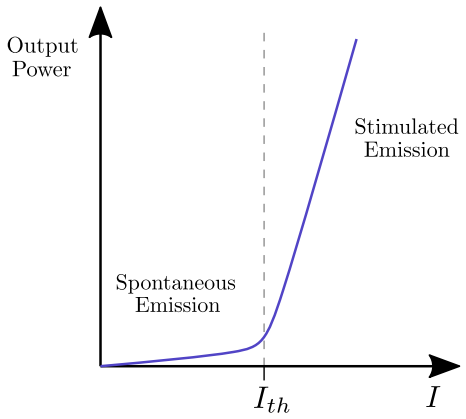

Figure 3.9: Output power of a laser diode against injection current. Above I_{th} stimulated emission starts to dominate

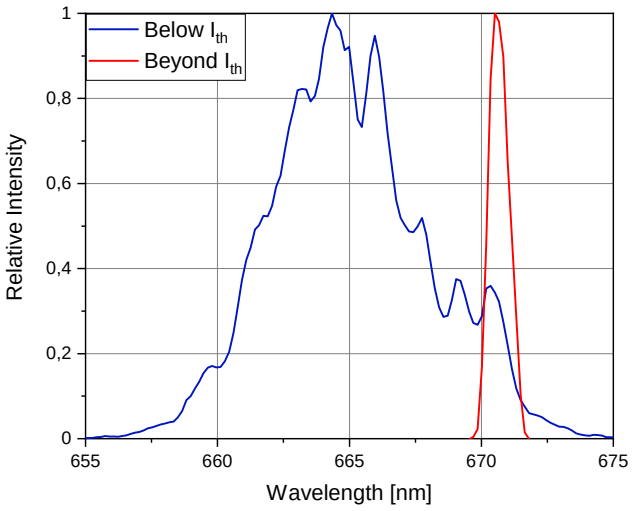

Figure 3.10: Relative intensity of the DL pro below I_{th} compared to the carrier peak at $\lambda = 671$ nm

3.3.2 Phase noise

The main advantage of an OPLL compared to conventional frequency stabilization, which does not take the phase of the signal into account, becomes clear when looking at the power spectrum. In the Figure 3.11 one can see an unlocked signal (blue), in which a frequency lock may shift the signal to the correct frequency but the shape remains unchanged. A significant portion of the power is in frequencies outside the carrier frequency. So this stabilization does not affect the noise. However, if we now consider the power spectrum with additional phase stabilization (red), noise around the carrier frequency is strongly suppressed and most of the power is contained in the carrier. With help of phase stabilization, a very low-noise signal can be generated, being very useful for applications in which phase coherence plays a decisive role.

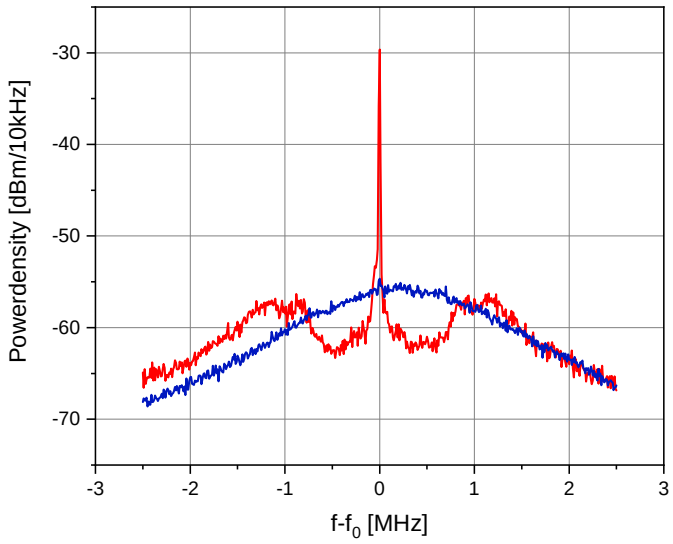

Figure 3.11: Shape of the beat signal with (red) and without phase locking (blue). Phase locking suppresses noise around the carrier and most of the power is contained in the carrier

An ideal sinusoidal signal would have a delta function as the power spectrum. However, every signal is subject to processes that lead to a deviation from the desired frequency. This leads to a blurred out spectrum around f_0. Let us consider the beat signal in the presence of noise.

$$E(t) = [E_0 + A(t)] \sin(2\pi f_0 t + \phi(t)) \tag{3.21}$$

Where $A(t)$ denotes the amplitude and $\phi(t)$ the phase noise. In our discussion of the power spectrum, we neglect the amplitude noise. However, this is not irrelevant for driving Raman transitions. Amplitude fluctuations correspond to intensity changes, which

in turn, because of (2.8), lead to an undesired change in Rabi frequency.

In the rest of this section, we will discuss the propagation of phase noise in an OPLL following [12], which will ultimately explain the shape of the beat signal in figure 3.11.

In order to discuss noise the Power Spectral density is (PSD) analysed. Therefore the Fourier transform is usually calculated. Random stationary fluctuations however are in general not square integrable, thus the energy $||E||_2^2$, where $||.||_2^2$ is the L^2- norm, or the Fourier transform $\mathcal{F}\{E(t)\}$ in general do not exist. In this case time limited parts E_T of the signal are considered

$$E_T(t) = \begin{cases} E(t), & t \in [-T, T] \\ 0, & t \notin [-T, T] \end{cases} \tag{3.22}$$

The average power during the interval $[-T, T]$ is then

$$\frac{1}{2T} \int_{\mathbb{R}} |E_T(t)|^2 \, dt = \frac{1}{2T} \int_{\mathbb{R}} |\mathcal{F}\{E_T(t)\}(\omega)|^2 \, d\omega \tag{3.23}$$

where equality to the integral over the Fourier transform is given by Plancherels theorem. If we now demand that the average power of the signal is finite

$$\lim_{T\to\infty} \frac{1}{2T} \int_{\mathbb{R}} |E_T(t)|^2 \, dt < \infty \tag{3.24}$$

we can define the PSD $S_E(\omega)$:

$$S_E(\omega) = \lim_{T\to\infty} \frac{1}{2T} |\mathcal{F}\{E_T(t)\}(\omega)|^2 \tag{3.25}$$

The PSD is often defined as Fourier transform of the autocorrelation function

$$S_E(\omega) = \mathcal{F}\{r_E(t)\}(\omega) = \frac{1}{2\pi} \int_{\mathbb{R}} r_E(t) \exp(-i\omega t) \, dt \tag{3.26}$$

where $r_E(t)$

$$r_E(t) = \frac{1}{2T} \int_{-T}^{T} E(t) E^*(t+\tau) \, d\tau \tag{3.27}$$

is the autocorrelation function of the signal $E(t)$. The equality to the definition above is given by the Wiener–Khinchin theorem.

For LTI systems noise with spectrum $S_{Noise}(\omega)$ propagates as follows

$$S_{\text{Noise, out}}(\omega) = |H(\omega)|^2 \, S_{\text{Noise, in}}(\omega) \tag{3.28}$$

where $H(\omega)$ is the noise transfer function. What does this mean for our OPLL? In order to see how the noisy beat signal is changed by the phase lock, we have to determine

the transfer function and spectral power density of the noise. In case of active phase stabilization, we thus have:

$$S_{\text{Beat noise, locked}}(\omega) = |H(\omega)|^2 \, S_{\text{Beat noise, unlocked}}(\omega) \tag{3.29}$$

The PSD $S_E(f)$ from the signal in (3.21) can be calculated using the equations above and is given by

$$S_E(f) = E_0^2 \left[(1-\sigma_\phi^2)\delta(f-f_0) + S_\phi(f-f_0)\right] \tag{3.30}$$

where $S_\phi(f-f_0)$ is the phase noise power spectral density of which the variance is given by

$$\sigma_\phi^2 = \int_{-\infty}^{\infty} S_\phi(f)\, df \tag{3.31}$$

For a detailed calculation see [12]. The carrier only contains a fraction $1-\sigma_\phi^2$ of the total power, the rest is distributed around f_0 described by $S_\phi(f)$. Since the spectrum in general is symmetric around f_0 one is usually interested in the single-sided phase noise, which describes the noise power in a bandwidth of 1 Hz at f relative to the power in the carrier at f_0. It is common to use the unit dBc/Hz (dB carrier, dB relative to carrier power) or rad^2/Hz. Experimentally this is determined by measuring the power $P(f)$ using a spectrum analyser

$$S_\phi(f) = \frac{10^{\frac{P_E(f-f_0)}{10}}}{\text{RBW} \cdot 10^{\frac{P_E(f_0)}{10}}} \tag{3.32}$$

where RBW is the resolution bandwidth of the spectrum analyser. The ratio between carrier to total power is given by:

$$\eta = \frac{S_E(f_0)}{\int_{-\infty}^{\infty} S_E(f)\, df} \tag{3.33}$$

The relation beween η and the phase noise variance is given by $\eta = 1-\sigma_\phi^2$ as one can see from equation (3.30).

Each component in the loop is a source of noise. The VCO consisting of both lasers however is the dominant noise source, with noise transfer function:

$$H(s)_{\text{VCO}} = \frac{1}{1+G(s)} \tag{3.34}$$

With equation (3.29) we get an expression describing how the beat noise propagates in the OPLL,

$$S_{\phi,\text{locked}}(f) = \left|\frac{1}{1+G(s)}\right|^2_{s=2\pi i f} \underbrace{[S_{\phi,\text{M}}(f) + S_{\phi,\text{S}}(f)]}_{S_{\phi,\text{unlocked}}} \tag{3.35}$$

Where $S_{\phi,\text{M}}(f)$ and $S_{\phi,\text{S}}(f)$ are the phase noise of Master and Slave laser respectively. The open loop gain $G(s)$ can be approximated by

$$G(2\pi i f) = K\frac{e^{2\pi i f \tau}}{if} \tag{3.36}$$

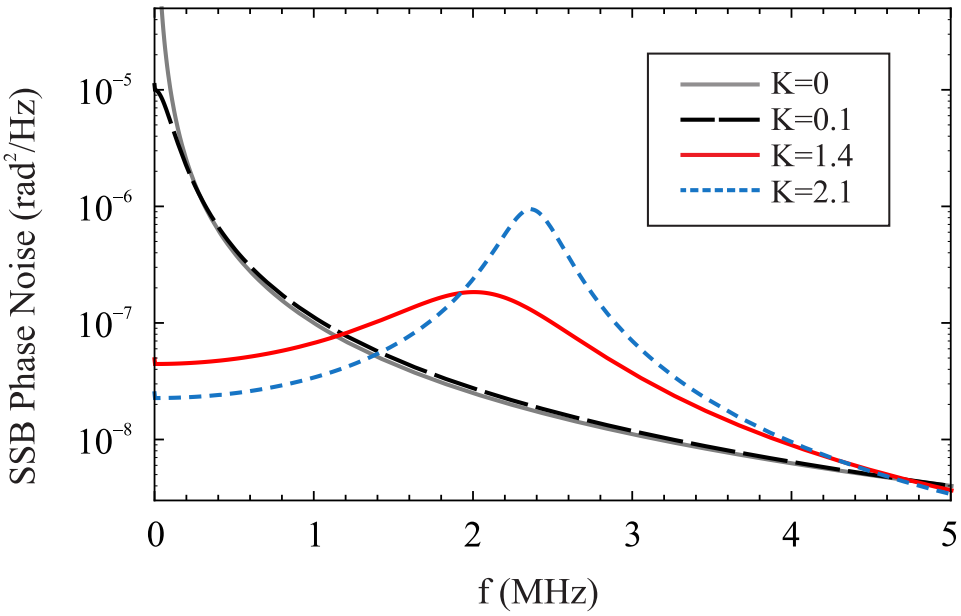

Figure 3.12: $S_{\phi,\text{locked}}(f)$ for different gain values K. If we increase the gain, noise around the carrier is strongly suppressed and the servo bumps arise. Taken from [12].

where K is the overall linear gain. Assuming the unlocked noise of both lasers can be modelled as a superposition of white and $1/f$ frequency noise we get

$$S_{\phi,\text{unlocked}}(f) = (2\pi)^2 \left[C_w + \frac{C_{1/f}}{2\pi f} \right] \tag{3.37}$$

where C_w and $C_{1/f}$ are coefficients for each noise. Plugging (3.36) and (3.37) into (3.35) yields:

$$S_{\phi,\text{locked}}(f) = \frac{1}{f^2} \left| \frac{if}{if + Ke^{2\pi i f \tau}} \right|^2 (2\pi)^2 \left[C_w + \frac{C_{1/f}}{2\pi f} \right] \tag{3.38}$$

Figure 3.12 shows $S_{\phi,\text{locked}}(f)$ for different gain values. If we increase the gain, noise around the carrier is strongly suppressed and the servo bumps arise, which in combination with a delta peak leads to the shape of the beat in figure 3.11.

4 Experimental Setup

4.1 Already existing Setup

This section gives a brief overview of the experimental setup for preparation of ultracold Lithium atoms. More detailed information on the cooling processes can be found in the literature ([13], [14], [6]). Further information of our experimental setup can be found in several theses from our group ([15], [16], [17], [18]).

All experiments with ultracold atoms have to be performed in ultra high vacuum, otherwise collisions with the background gas would lead to very short lifetime of the trapped atoms, which makes experiments impossible. Figure shows the vacuum chamber with several pumps (1),(2) ensuring a pressure in the order of 10^{-12} mbar at the position where the atoms are trapped [15]. Fist the ^{6}Li atoms are heated in a oven to around

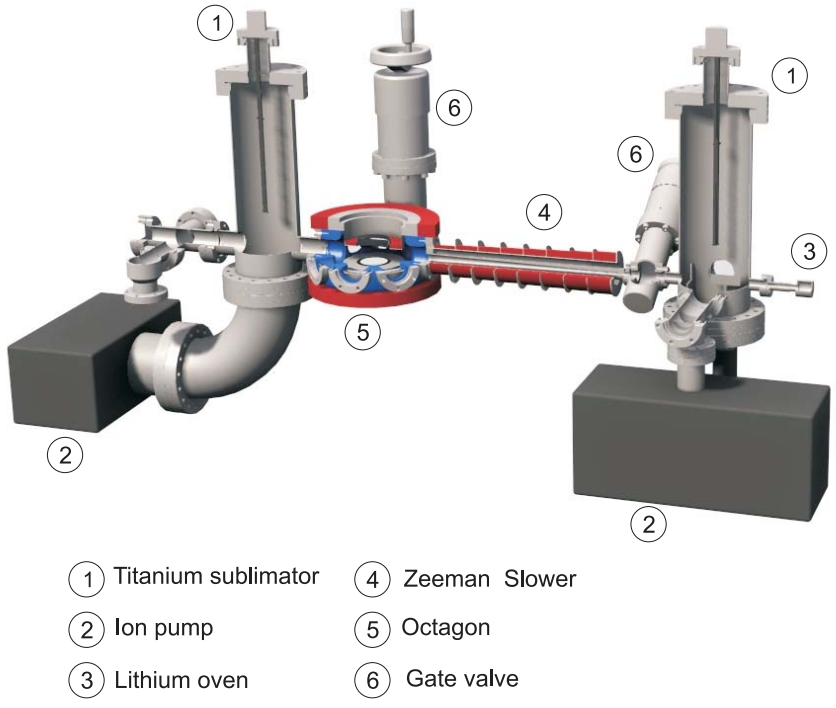

Figure 4.1: Vacuum chamber. After leaving the oven (3) the atoms are slowed down by the Zeeman slower (4) and then trapped by an MOT in the octagon (5), where they are transferred into a dipole trap. Taken from [15].

360°C and slowed down by the **Zeeman Slower** from a initial velocity of 800 m/s to

60 m/s [17]. This is achieved with a counterpropagating laser beam resonant to the D_2 line ($\lambda \approx 671$ nm). When absorbing a photon from the beam total momentum is conserved, reducing the atoms momentum by $p = h/\lambda$ with each absorption. Since the spontaneous emitted photons do not prefer a spatial direction this results in a net force decelerating the atoms. To compensate the Doppler shift a magnetic field is applied with decreasing strength in direction of the octagon.

The next step is further cooling and trapping by a **MOT** (magneto-optical-trap). The Zeeman slower is needed to reduce the velocity of the atoms to a range where they can be captured by a MOT. Two separate mechanisms act in a MOT, one to cool the atoms, the other to trap them at a certain position. The cooling is achieved by three pairs of counterpropagating beams red-detuned from resonance, each of which is orthogonal to one another. If an atom is now moving, the beam directed against the movement appears blue shifted due to the Doppler effect. The detuning Δ is reduced to $\Delta - \mathbf{k} \cdot \mathbf{v}$. It is therefore more likely that a photon will be absorbed against direction of movement and the momentum transfer will reduce the velocity. A Taylorexpansion of the force for small velocities yields $\mathbf{F} = -\delta\mathbf{v}$, with constant δ [13]. This is analogous to viscous damping in mechanics and therefore also known as optical molasses. Since the Doppler effect plays an important role this process is called Doppler cooling. The lowest temperature that can be reached with Dopplercooling, the so-called Doppler limit, is

$$T_D = \frac{\hbar\Gamma}{2k_B} \tag{4.1}$$

For ^{6}Li the Doppler limit is 140 μK [15]. With an optical molasses it is possible to cool the atoms, but the force only depends on the velocity and not on the position, i.e. in order to trap the atoms in a certain area,an additional position-dependent force is necessary. This can be achieved by applying a magnetic quadruple field in addition to the optical molasses. Near the center the magnetic quadrupole field is linear in each spatial direction, therefore the energy splitting of the atomic lines is also linear. The right choice of polarization of the red-detuned laser beams now ensures a resorting force $\mathbf{F} = -\delta\mathbf{v} - k\mathbf{x}$ [13]. This is analogous to the restoring force in a spring with an additional friction term.

The temperature is still too high to prepare a few atom system. Further reduction through evaporative cooling in a **dipole trap** follows. The idea is to transfer atoms from the MOT to a conservative potential and remove the hot atoms, while the remaining rethermalize. This is similar to cooling of a hot cup of tea. An optical dipole trap set up by a focused laser beam provides a nearly conservative potential. The electric field of the laser induces a dipole moment on the atom $\mathbf{p} = \alpha\mathbf{E}$, where α is the polarizability of the atoms. The potential energy of this dipole in the electric field is given by [19]

$$U_{\mathrm{dip}}(\mathbf{r}) = -\frac{3\pi c^2}{2\omega_0^3}\left(\frac{\Gamma}{\omega_0 - \omega} + \frac{\Gamma}{\omega_0 + \omega}\right) I(\mathbf{r}) \tag{4.2}$$

where ω_0 is the resonance frequency, ω the laser frequency and Γ the linewidth. The potential is proportional to the beam intensity. Our dipole trap is realized with a far red detuned $\lambda = 1064$ nm laser with maximum power of $P = 200$ W. By slightly decreasing the overall intensity and thus lowering the trap depth, the atoms with highest kinetic energy can escape, allowing the remaining to rethermalize. With this technique we can prepare 40.000 atoms with a temperature of 250 nK [16].

Now a second 1064 nm laser is focused on the dipole trap creating the **micro trap**. This beam has a waist of 1.15 μm [18]. This tightly focused beam in combination with the large dipole trap results in a potential shown in figure 4.2. With this trick we create a highly degenerate Fermi gas with occupation probability of nearly 1 for the lowest states. After the states in the micro trap are populated the larger dipole trap is switched of

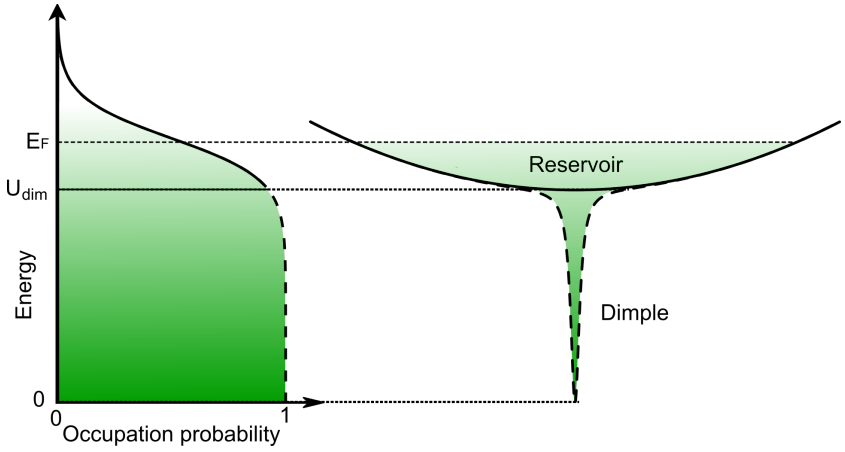

Figure 4.2: A tightly focused beam with waist of 1.15 μm is superimposed to the dipole trap, creating the micro trap with high occupation probability for the lowest levels. Taken from [16].

leaving us with around 1000 atoms in the micro trap [17].

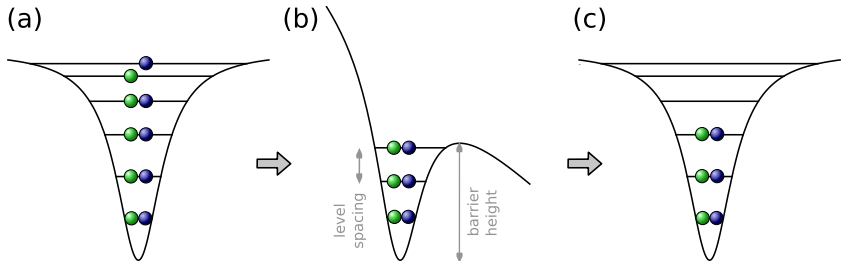

Figure 4.3: Spilling in the micro trap. A magnetic field gradient lowers the trap, allowing the highest atoms to escape. Taken from [16].

The last step to lower temperature and atom number is the **spilling** technique. By adding a magnetic field gradient one side of the potential is lowered and the highest

atoms can escape. After spilling the magnetic field gradient is switched off, restoring the initial micro trap.
For imaging the atoms after performing the experiment we recapture them in a MOT, called μMOT. The beams of the μMOT excite the atoms and the fluorescence signal is focused onto a CCD camera. The intensity of the signal is proportional to the atom number, allowing us to determine how many atoms are captured in the trap.

4.2 Phase Lock Setup

In our setup we use two external cavity diode lasers, the DL pro and DL 100 from the manufacturer Toptica. Both lasers have a center frequency of $\lambda = 671$ nm. We will use the DL pro as a slave and the DL 100 as a master laser. After light from the DL pro passes a $\lambda/2$ plate, it is split into two beams by a PBS cube, one of which goes to the second part of the setup, in which both lasers, the DL pro and DL 100 also referred as Pump and Stokes laser, respectively, are combined and guided to the atoms, while the other is brought together with light from the DL 100 by a Fiber Beam Splitter from Thorlabs with a 50:50 coupling ratio. We use one with reduced length to around 30 cm, instead of the standard commercially available with length of a meter in order to reduce the time delay of the optical feedback loop. Since the light only propagates with $2/3c_0$ in the fiber, its length mainly determines the time delay τ of our loop. The beat signal is now coming out at both outputs of the Fiber Beam Splitter.

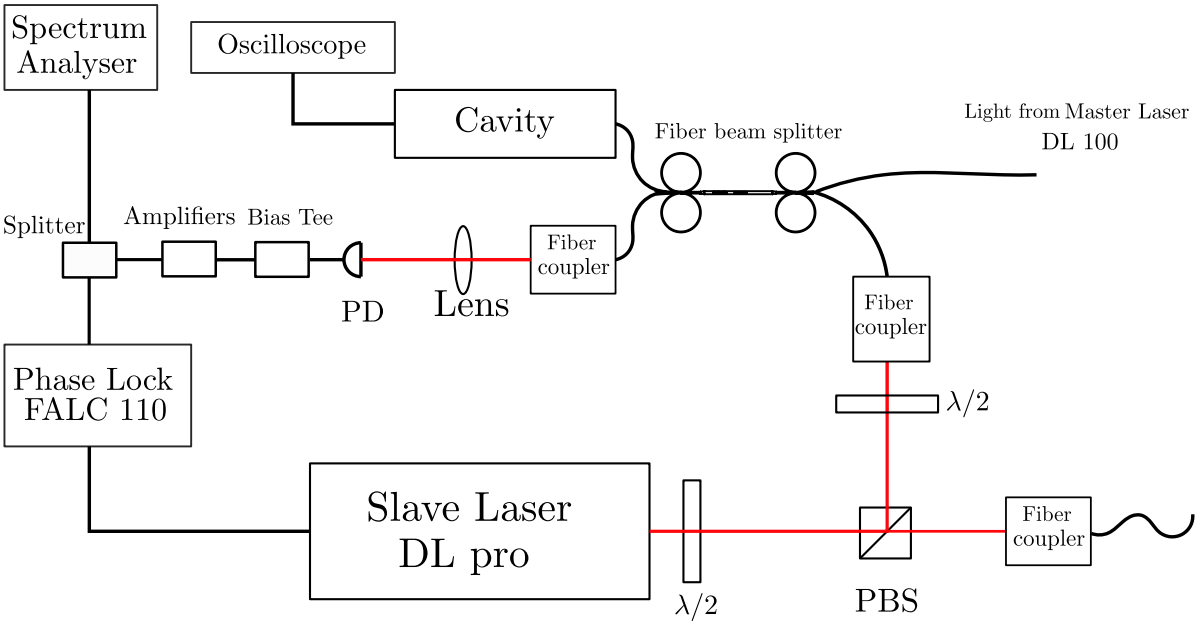

Figure 4.4: Setup for phase locking the DL pro

One output is connected to a cavity. We use a Scanning Fabry Perot Interferometer from Thorlabs. This spectrum analyser only transmits specific frequencies, which can

be tuned by changing the length of the cavity by a piezo. The transmitted light is then detected by a photodiode and displayed on an oscilloscope.
The cavity is mainly used for diagnosis reasons. For instance we noticed that the DL pro was not running single mode at certain currents values near I= 45 mA. This can be seen on the oscilloscope connected to the cavity and should be avoided in experiment.

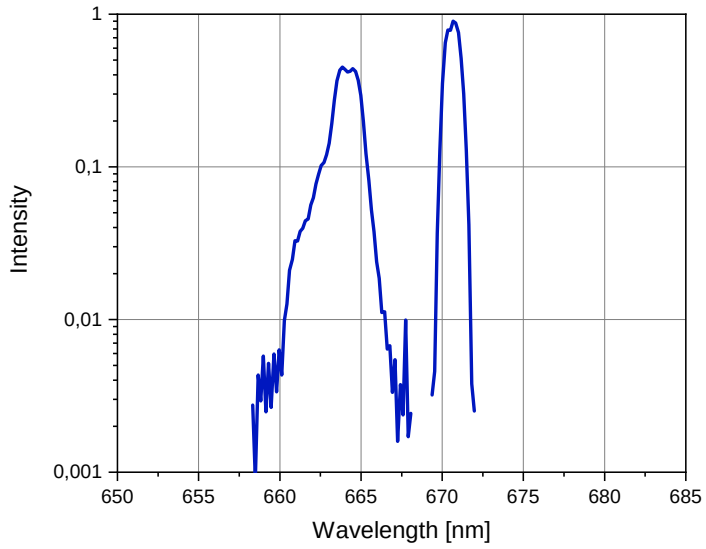

Figure 4.5: DL pro not running single mode for currents around I=45 mA. There is an undesired amplification at $\lambda = 664$ nm. Mode selection by the grating does not work properly here.

Light from the other output is focused on a photodiode with a lens, whereupon a Bias Tee cuts off the DC part followed by three amplifiers. One part is split off and sent to the Rohde and Schwarz spectrum analyser where we can observe the beat signal, the other part is sent to our OPLL module, the Toptica FALC 110, which now regulates the DL Pro. Two different control mechanisms are possible here. The current and voltage regulation. Direct regulation of the diode current has a bandwidth of several Mhz and is necessary for fast regulation such as phase locks, while additional voltage regulation of the grating piezo has a bandwidth of a few 10 kHz and cancels out long-term frequency drifts. In order to phase lock properly the beam on the photodiode should have a power of 1 mW.

In the second part of the setup, both beams are sent through an acousto-optical modulator (AOM). It allows us to give pulses of different time durations to the atoms and to control the beam power . In an AOM, a piezo oscillator produces sound waves, usually in the radio frequency range. These sound waves cause a periodic change in the crystal

density and thus also a periodic change in the refractive index, which diffracts the incoming beam. The light leaves the AOM in different orders $m \in \mathbb{Z}$, each at a different angle θ_m and frequency $f_0 + mF$, with the frequency shift F equal to the frequency of the sound wave. We use a AOM with a frequency of $F = 80$ MHz. For the experiment we use the order $m = 1$. Note that the frequency shift caused by the AOM does not affect the beat frequency, since both beams are shifted by 80 MHz the frequency difference stays the same.

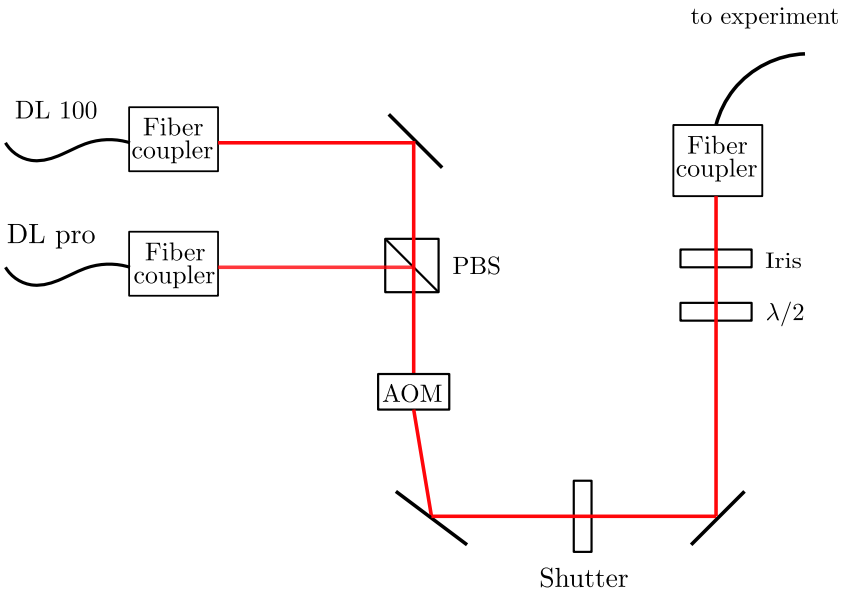

Figure 4.6: Setup for guiding both beams to the atoms

Component	Model no.	Manufacturer
Slave Laser	DL pro	Toptica Photonics
Master Laser	DL 100	Toptica Photonics
Phase Lock	FALC 110	Toptica Photonics
Spectrum Analyser	FSL 9kHz...6GHz	Rohde & Schwarz
Fabry Perot Cavity	SA200-5B	Thorlabs
Fiber beam splitter	PN670R5A2	Thorlabs
Photo diode	G4176	Hamamatsu
Bias Tee	ZX85-12G-S+	Mini-circuits
Amplifiers	ZX60-14012L-S+	Mini-circuits
Splitter	ZX30-17-5-S+	Mini-circuits
AOM	AOMO 3080-120	Gooch & Housego

Table 4.1: Components used in the phase lock setup

For additional mechanical control a shutter is placed after the AOM. The beams then passes a $\lambda/2$ plat and a Iris, that blocks other orders than the first. This is not to

prevent other orders to be coupled into the fiber, which would not happen since they are spatially separated, but it makes working with the setup easier. Coupled into the fiber the beam is finally lead to the trapped ^{6}Li atoms.

5 Measurements

5.1 Incoherent background of the DL pro

The spectrum of the Toptica DL pro laser was recorded using the Tohrlab CCS175/M, which is a CCD spectrometer with a wavelength range from 500 nm to 1000 nm. We are particularly interested in the incoherent background. That is why we reduce the current until the carrier peak at 671 nm can no longer be seen. If we now increase the current

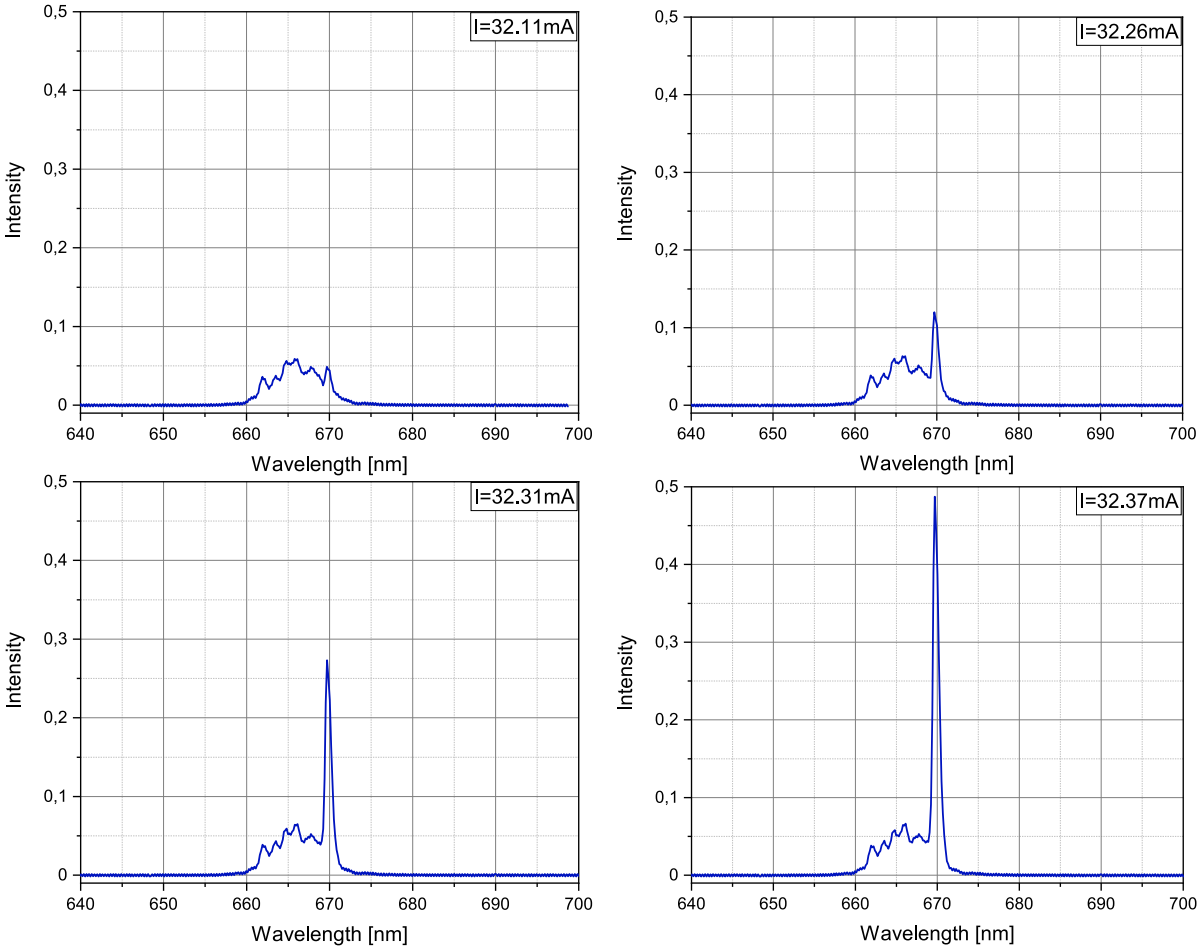

Figure 5.1: Spectra of the Toptica DL pro Laser passing the threshold current. The incoherent background remains constant, while the resonant mode increases linearly with the current.

in small steps, we see that the intensity of the incoherent background increases until the

laser threshold I_{th} is reached. From here on, the intensity of the background remains the same, while that of the peak increases linearly.

By looking at the spectrum, the threshold current was determined to be $I_{th} = (31.6 \pm 0.1)$ mA. A small peak resulting from stimulated emission can already be seen in the upper left spectrum. Note that even in the bottom right spectrum the laser is running on a much lower current than usual. The power in the carrier peak is significantly larger for typical currents of 40-50 mA. Unfortunately spectra with higher current could not be taken without further adjustments. The main limitation was the dynamical range of the CCD spectrometer used. A higher current would lead to a saturated spectrum. Special care should be taken when interpreting and recording the data. If one wants to determine the ratio of power in the incoherent background to power in the carrier $P_{\mathrm{IB}}/P_{\mathrm{C}}$ for high currents ($\sim$ 50 mA) based on the spectrum, the light must first be dimmed such that the spectrum is no longer saturated. Although the power that goes into the fiber is now reduced, the ratio of power in the background to power in the carrier remains high. It turns out that it is so high that no photons are detected in the incoherent background region and the power ratio can not be determined using the CCD spectrometer. Another inaccuracy that has to be taken into account when calculating ratios from the spectrum is that the spectrometer does not scale linearly with integration time. For different integrations times ratios of certain areas in spectrum were off by a factor of 2.

But why are we interested in the background at all? If we prepare an ensemble of atoms in a dipole trap and expose them to a laser beam, the scattering rate consists of the contribution from carrier and background:

$$\Gamma_{\mathrm{sc}} = \Gamma_{\mathrm{IB}} + \Gamma_{\mathrm{C}} \tag{5.1}$$

The scattering rate of the carrier that is detuned from resonance cannot be changed and is given by (2.24). The incoherent background is now distributed over a wide range of frequencies. We are particularly concerned about the part that is on resonance, eventually causing high scattering rates.

While the power of stimulated photons increases the incoherent background resulting from spontaneous emitted ones however stays the same. What does that mean for our purpose? Even though we can not reduce the spontaneously emitted photons we can still increase the ratio between power in the main carrier and power in the incoherent background by using high currents and thus minimize the relative contribution of the background. We therefore set the current to roughly 52 mA, with the upper limit of the DL pro being 55 mA.

The ratio $P_{\mathrm{IB}}/P_{\mathrm{C}}$ was determined by placing a powermeter behind the $\lambda/2$ plate in front of the DL pro. $P_{\mathrm{IB}} = 0.5$ mW was measured for $I = 31.6$ mA and $P_{\mathrm{total}} = 25.9$ mW for

$I = 52.32$ mA. We obtain

$$\frac{P_{\mathrm{IB}}}{P_{\mathrm{C}}} = \frac{P_{\mathrm{IB}}}{P_{\mathrm{total}} - P_{\mathrm{IB}}} \approx 2\% \tag{5.2}$$

The contribution of incoherent background to scattering rate can be determined as follows. At first, atoms are prepared in the micro trap, which is then exposed to a a laser beam. The number of atoms decays exponentially and the lifetime T can be determined, of which the inverse $\Gamma = 1/T$ yields the scattering rate. Now one measures the lifetime T_{total} for a typical high current as used in the experiment, then the current is turned down to I_{th} and the lifetime T_{IB} is measured again. From this, the scattering rates of the carrier and background can be calculated,

$$\begin{aligned} \Gamma_{\mathrm{total}} &= \frac{1}{T_{\mathrm{total}}} \\ &= \underbrace{\frac{1}{T_{\mathrm{IB}}}}_{\Gamma_{\mathrm{IB}}} + \underbrace{\left(\frac{1}{T_{\mathrm{total}}} - \frac{1}{T_{\mathrm{IB}}}\right)}_{\Gamma_{\mathrm{C}}} \end{aligned} \tag{5.3}$$

as well as the relative influence of the background .

$$\frac{\Gamma_{\mathrm{IB}}}{\Gamma_{\mathrm{total}}} = \frac{T_{\mathrm{total}}}{T_{\mathrm{IB}}} \tag{5.4}$$

5.2 Performance of the OPLL

We phase lock our lasers with the Toptica FALC 110 and record the power spectrum of the beat signal for different frequencies with the Rohde and Schwarz spectrum analyser. The spectra were recorded with a resolution bandwidth of 10 kHz, video bandwidth of 100 Hz and sweep time of 5.2 s over a range of 5 MHz.

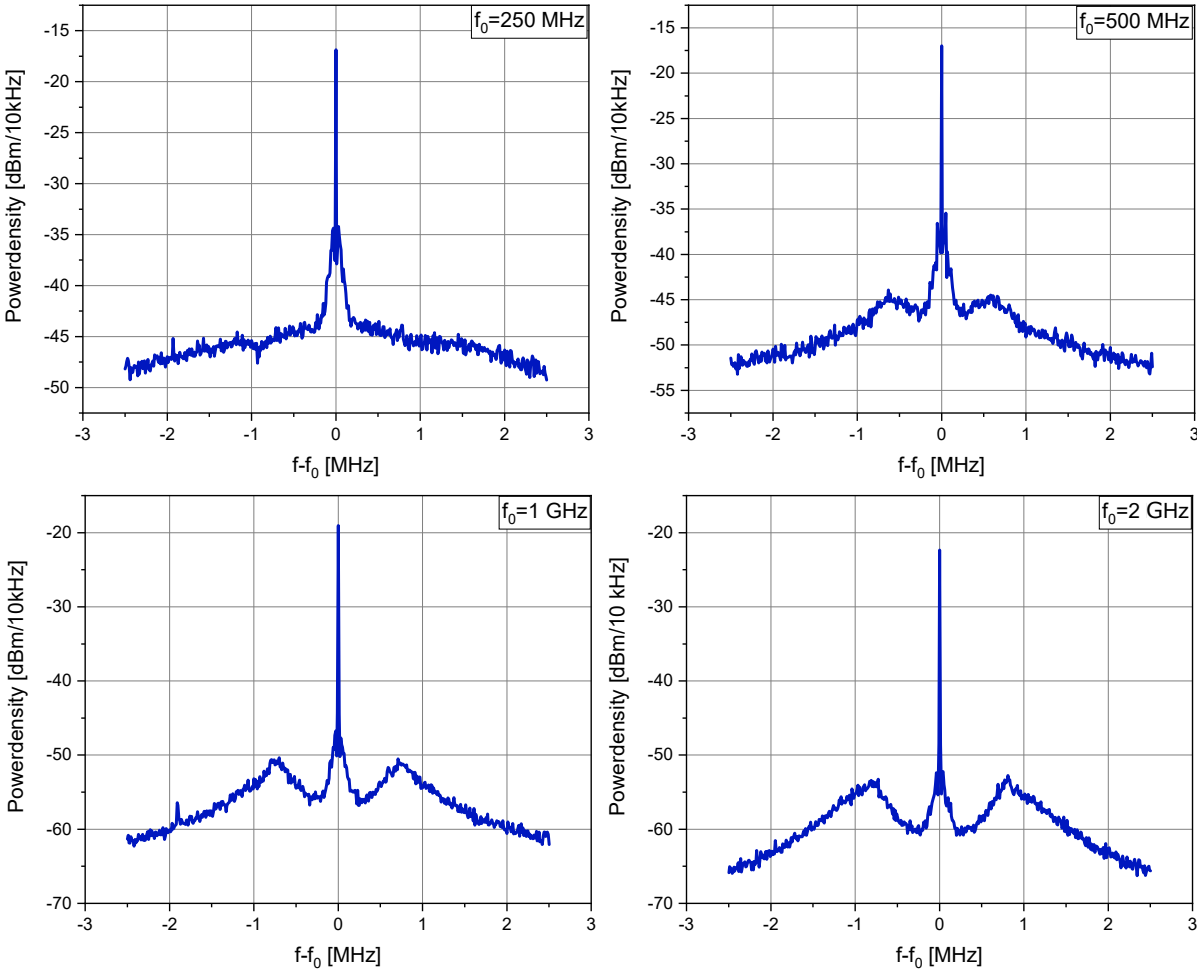

Figure 5.2: Beat signals for different frequencies. Characteristic for a phase locked laser is the narrow carrier.

One of the most important characteristics when evaluating performance of the loop is the ratio between power in carrier to overall power. We calculate the ratios, by integrating the spectra in the carrier region and dividing by the integral over the complete spectrum. Furthermore we roughly determine the position of the servo bumps. For $f_0 = 250$ MHz there are no bums visible. While the lock provides satisfactory results for $f_0 = 1$ GHz and above, the performance for lower frequencies might not be sufficient for applications where this range is needed. This however does not affect the Raman transitions we want

to drive, since the beat frequency will be between 1 GHz and 2 GHz.

f_0[GHz]	$P_{\text{carrier}}/P_{\text{total}}$ [%]	$f_{\text{servo bumps}}$ [MHz]
0.25	55	
0.5	67	0.6
1	89	0.7
2	89	0.8

Table 5.1: Power in carrier and position of servo bumps for different beat frequencies

5.3 Rabi Oscillations

We want to drive Raman transitions between state $|3\rangle$ and $|4\rangle$ at B=685 G, where $|3\rangle$ is the initial state. Calculating the Raman rates according to [8], there are only two possible pairs of polarisation (q_P, q_S) for the Pump and Stokes laser in order to drive this transition:

$$(q_P, q_S) = \begin{cases} (\pi, \sigma^-) \\ (\sigma^+, \pi) \end{cases} \tag{5.5}$$

For other polarisations the Raman rate is zero. We will use the DL pro as Stokes and the DL 100 as Pump laser. We choose the polarisation (π, σ^-), since we expect higher a Rabi frequency based on calculations in [8].

The energy difference between state $|3\rangle$ and $|4\rangle$ at B=685 G is $E/\hbar = 2\pi \times 1.77381$ GHz at which the Raman laser is phase locked to the free running Stokes laser. In order to achieve large Rabi oscillations a collimated beam with beam diameter 4.3 mm is focused with a $f = 300$mm lens onto the atoms. Assuming a Gaussian beam this leads to a center waist of 30 μm. It is however highly doubtable that we actually hit the atoms with this waist. The actual waist and intensities of the beams can be calculated by measuring the Rabi frequency. For now lets assume we hit the atoms with a beam waist of 30 μm. The intensity of a Gaussian beam is given by

$$I = \frac{2P}{\pi \mathrm{w}^2} \tag{5.6}$$

where w is the waist. With the powers used in the experiment of $P_{\text{Pump}} = 0.7$ mW and $P_{\text{Stokes}} = 1.7$ mW we obtain

$$\begin{aligned} I_{\text{Pump}} &= 49.5\text{W/cm2} \\ I_{\text{Stokes, eff}} = \frac{1}{2} I_{\text{Stokes}} &= 60.1\text{W/cm2} \end{aligned} \tag{5.7}$$

Why is there a factor of 1/2 for the Stokes beam intensity? Both beams are linearly polarized. The Pump beam oscillates in direction of the magnetic field and thus is π

polarized, whereas the Stokes beam oscillates perpendicular to the field and is therefore a superposition of equal amounts of σ^- and σ^+ polarisation, whereby the latter cannot be used to drive Raman transitions. Hence, the σ^+ component only contributes to inelastic scattering.

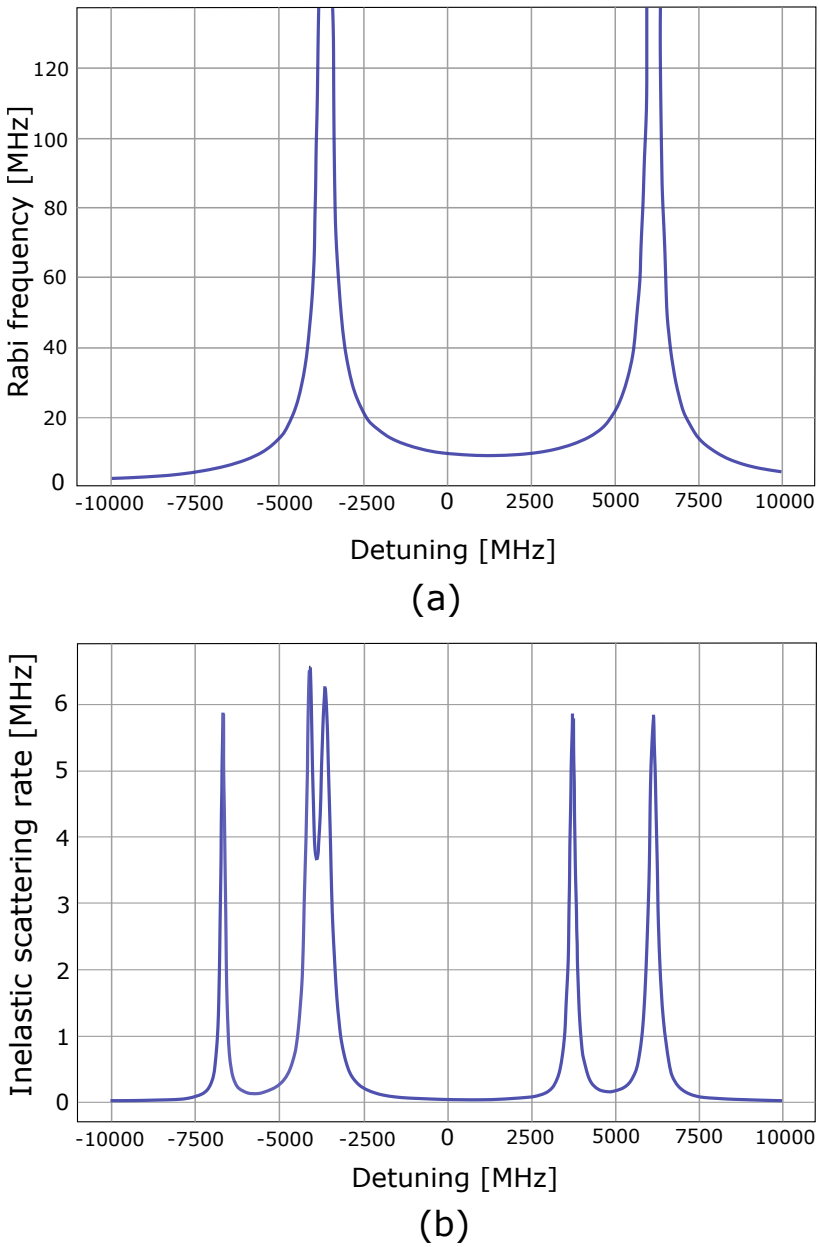

Figure 5.3: Expected Rabi frequency (a) and single photon scattering rate (b)

Now we still have to find the optimal detuning, such that $\beta = \Omega_R/\Gamma_{\text{sc}}$ is high. The Rabi frequency, single photon scattering rate and beta factor are calculated according to [8]. Figure 5.3 (a) shows the Rabi frequency for our waist and intensities. A detuning

of zero represents the D line without fine structure splitting. The peaks correspond to resonance with the D_1 or D_2 line. Here not only the Rabi frequency but also the scattering rate is high, which is shown in figure 5.3 (b).

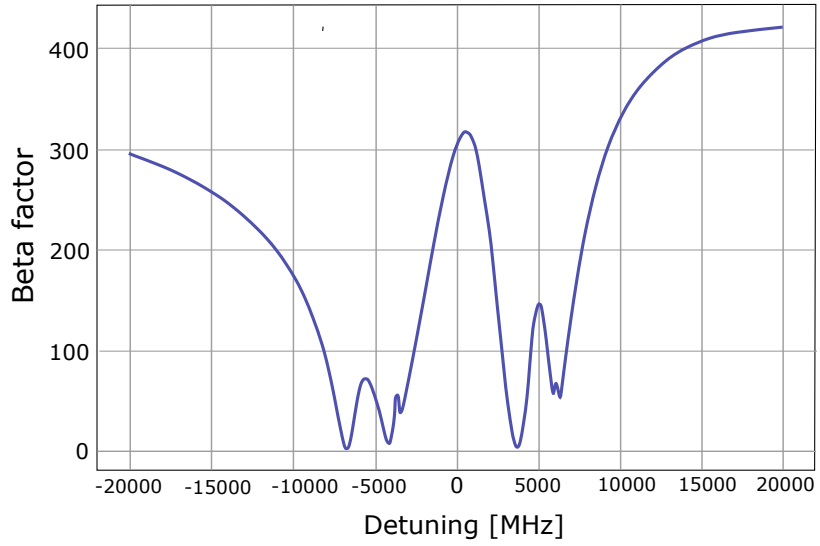

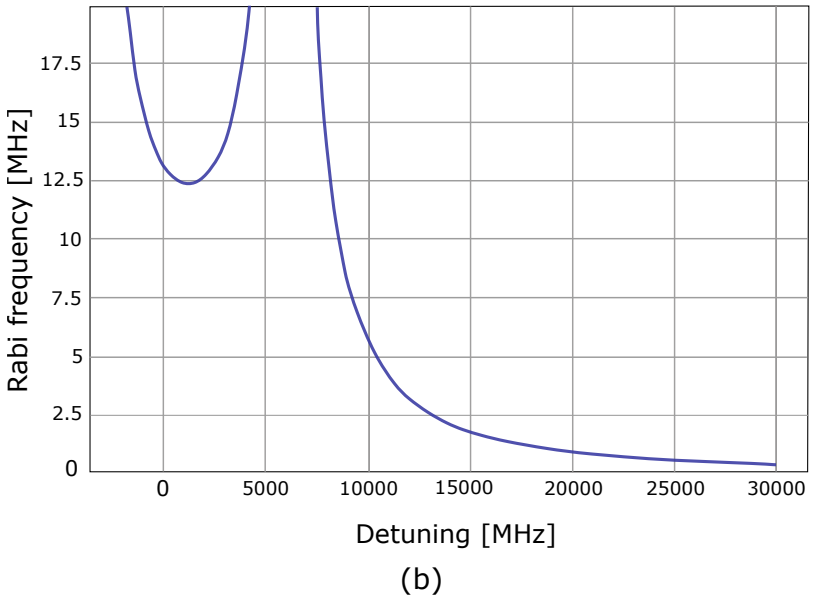

Figure 5.4: β factor (a) and Rabi frequency in between the D_1 and D_2 line and red detuned to both lines

The β factor is shown in figure 5.4 (a). We have high values between the D_1 and D_2 line, red detuned and blue detuned to both lines. Although the β factor is higher by a factor of roughly 1.3 in the red detuned region compared to in between the D lines, the Rabi frequency is lower by a factor of 0.1 as shown in figure 5.4 (b). One has to keep in

mind that we want fast oscillations, therefore not only the beta factor but also the Rabi frequncy has to be considered. For instance the beta factor is roughly the same for a detuning of 0 and 10 000 MHz, but the Rabi frequencies differ by a factor of two.
To achieve a high β factor, while maintaining fast Rabi oscillations we therefore choose our laser frequencies such that they are in between the D_2 and D_1 line. The frequency of the Pump laser is set to $\omega = 2\pi \times 446.7937$ THz. Figure 5.5 summarizes the configuration of both laser beams, where frequencies of the D_1 and D_2 line were assumed to be $\omega_{D_1} = 2\pi \times 446.789597791$ THz and $\omega_{D_2} = 2\pi \times 446.799650653$ THz according to [20].

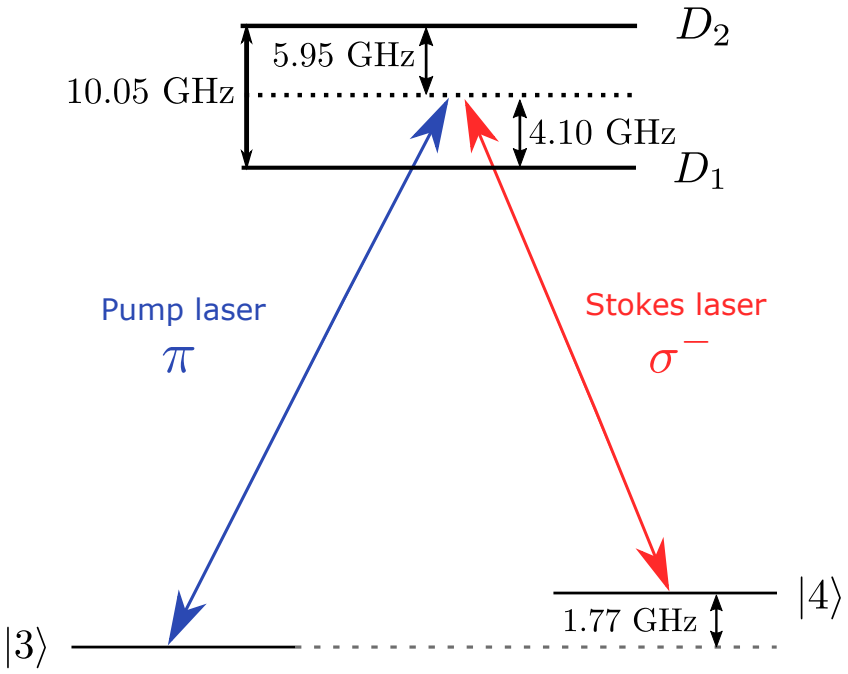

Figure 5.5: Configuration for driving Raman transitions between state $|3\rangle$ and $|4\rangle$ with B = 685 G. All frequencies given are optical

With these values we would expect a Rabi-frequency of 13 MHz.

Now we have to find the resonant magnetic field, i.e. the field such that the detuning δ from two photon resonance is zero. Looking at the formula for population in state $|4\rangle$

$$\left|c_{|4\rangle}(t)\right|^2 = \frac{\Omega_R^2}{\Omega_R^2 + \delta^2} \sin^2\left(\frac{\sqrt{\Omega_R^2 + \delta^2}}{2} t\right) \tag{5.8}$$

one might think that it does not matter or even is better if $\delta \neq 0$ since the Rabi frequency gets higher. But the amplitude simultaneously gets smaller. A complete population transfer is therefore only possible if $\delta = 0$.

We start with a $(|1\rangle, |3\rangle)$ mixture in the micro-trap. State $|1\rangle$ is shot out of the trap by resonant light, for which the field is increased to B=795 G beforehand. The reason

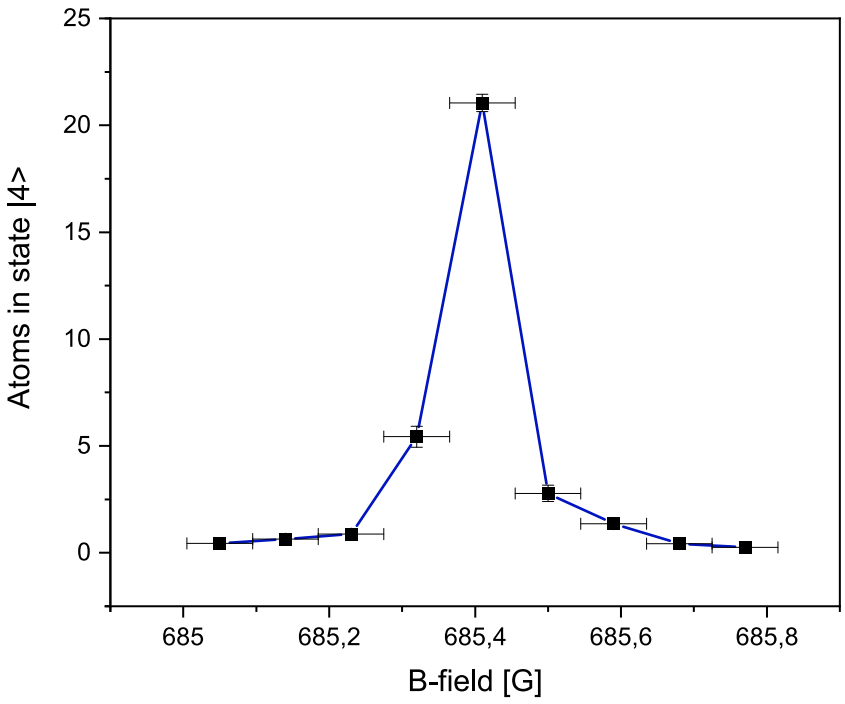

Figure 5.6: Atoms transferred to state $|4\rangle$ for different magnetic fields

for this is the weaker interaction between the two states than with 685 G. Too strong interaction when one state is shot out, could lead to a loss from atoms in the other state. The field is then reduced again to 685 G with only state $|3\rangle$ remaining trapped. The idea is now to send the Ramen beam to the atoms for a duration T, with which we achieve a population transfer in state $|4\rangle$. Then state $|3\rangle$ is shot out of the trap by resonant light. Only atoms in state $|4\rangle$ then remain. In order to ensure that the atoms which are left in the end are actually in this state, the Raman pulse can be omitted between the two shot outs, which leads to no atoms at all remaining.

First, the resonance was found by scanning the magnetic field while the exposure time of the two Raman beams is kept constant to $T = 2.5$ μs. The population transfer to state $|4\rangle$ is shown in figure 5.6. The error in magnetic field is due to the fact that we only have a magnetic field resolution of around 90 mG. The resonant magnetic field is chosen to B=685.4 G.

Now we measure the population of state $|4\rangle$ for different pulse durations and thus obtain Rabi oscillations.

The number of atoms in state $|4\rangle$ for a resonant transition is given by

$$N_{|4\rangle}(t) = N_{\max} \sin^2\left(\frac{\Omega_R}{2}t\right) \tag{5.9}$$

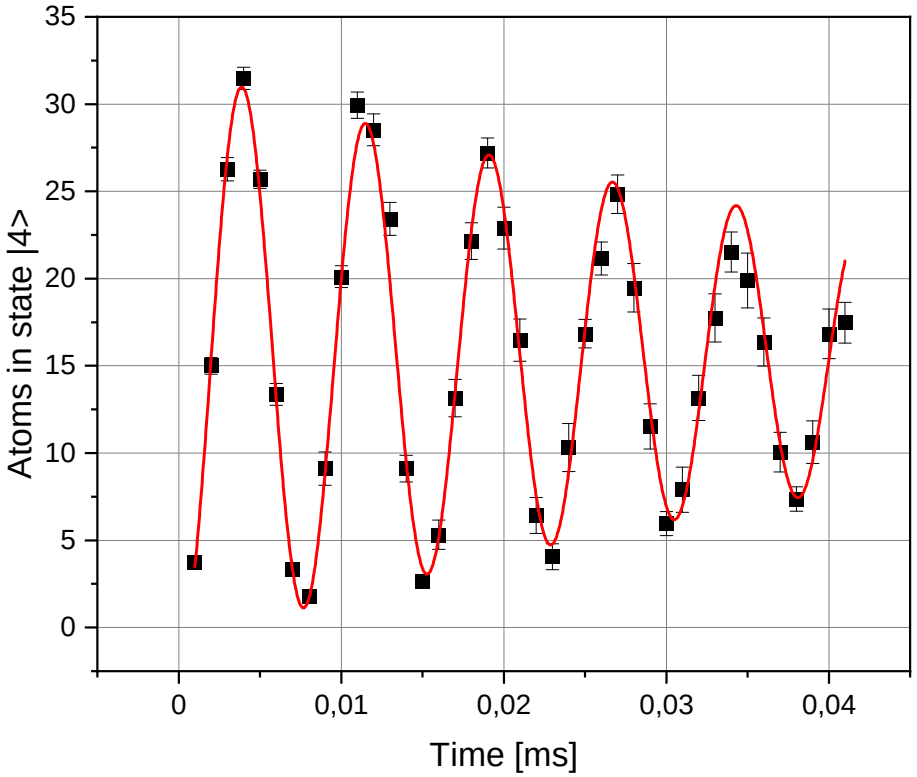

Figure 5.7: Rabi oscillations between state $|3\rangle$ and $|4\rangle$ at $\Omega_R = 2\pi \times (130.7 \pm 0.2)$ kHz

Using the identity $\sin^2(x) = \frac{1}{2}(1 - \cos(2x))$ we can rewrite this as

$$N_{|4\rangle}(t) = \frac{N_{\max}}{2}\left(1 - \cos\left(\Omega_R t\right)\right) \tag{5.10}$$

To accurately describe the measurement we modify this to

$$N_{|4\rangle}(t) = \frac{N_{\max}}{2}\left(1 - \cos\left(\Omega_R t\right)\exp\left(-\frac{t}{T}\right)\right) + N_0 \tag{5.11}$$

where the exponential describes the decoherence and N_0 the offset. Single photon scattering as well as magnetic field instability, which lead to phase fluctuations between laser and atoms, are decoherence sources. Fitting this function to the measured data yields a Rabi frequency Ω_R of

$$\Omega_R = 2\pi \times (130.7 \pm 0.2)\ \text{kHz} \tag{5.12}$$

Calculating back from this frequency we obtain a beam waist of 300 μm. We really do not hit the atoms with center waist.

5.4 Single Photon Scattering Rates

We measure the scattering rate for both lasers with same frequency and intensity values as when driving the Raman transitions with a magnetic field of B=685 G. First a $(|1\rangle, |3\rangle)$ mixture is prepared in the micro-trap, whereupon state $|1\rangle$ is shot out of the trap by resonant light. Then we measure the lifetimes of atoms in state $|3\rangle$ for both lasers one after the other.

We fit a exponential function to the data,

$$f(t) = A \exp\left(-\frac{t}{T}\right) \tag{5.13}$$

which yields the lifetimes:

$$\begin{aligned} T_{\text{Stokes}} &= (0.286 \pm 0.004)\ \text{ms} \\ T_{\text{Pump}} &= (2.59 \pm 0.04)\ \text{ms} \end{aligned} \tag{5.14}$$

For the Stokes laser the measured lifetime is significantly shorter, i.e. the scattering rate is higher than for the Pump. Reasons for this could on the one hand be the higher intensity $I_{\text{Stokes}}/I_{\text{Pump}} \approx 2.4$ and on the other hand that the Stokes laser is closer to the D_1 line. Since only state $|3\rangle$ is in the trap, detuning of the Pump laser to the D_1 line with 4.07 GHz is the same as when driving Raman transitions but the Stokes laser is now 1.77 GHz closer, resulting in a detuning of only 2.3 GHz.

Now the β factor can be calculated. The total scattering rate is given by

$$\begin{aligned} \Gamma_{\text{total}} &= \Gamma_{\text{Pump}} + \Gamma_{\text{Stokes}} \\ &= \frac{1}{T_{\text{Pump}}} + \frac{1}{T_{\text{Stokes}}} \end{aligned} \tag{5.15}$$

With our Rabi frequency of (130.7 ± 0.2) kHz this yields a beta factor of

$$\beta = (33.66 \pm 0.05) \tag{5.16}$$

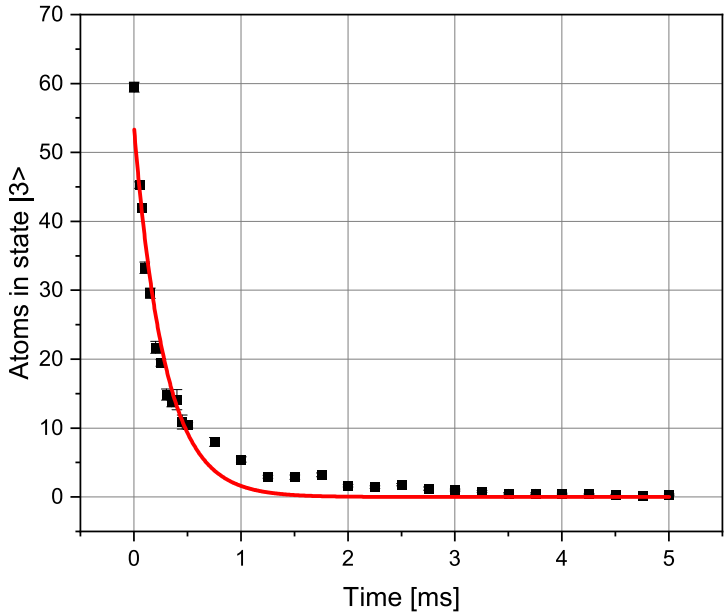

Figure 5.8: Lifetime measurement for the Stokes laser

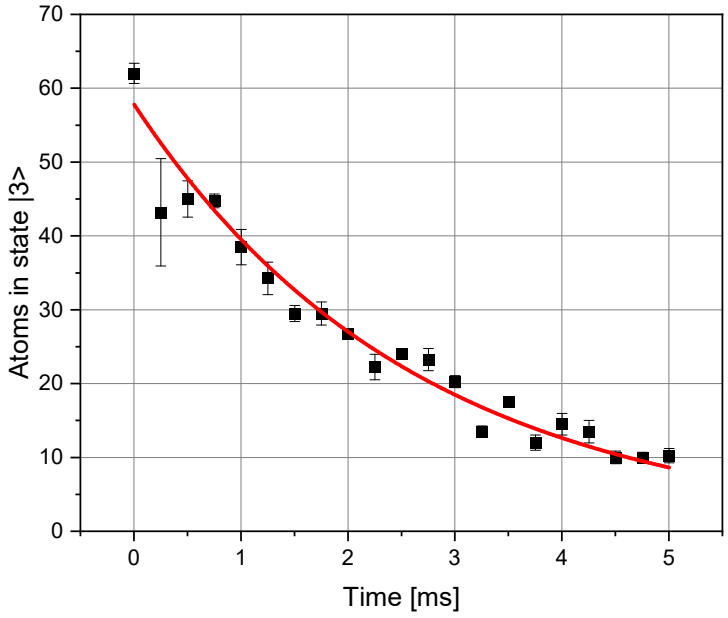

Figure 5.9: Lifetime measurement for the Pump laser

6 Conclusion and Outlook

We successfully performed Raman transitions between ground states $|3\rangle$ and $|4\rangle$ with a Rabi frequency of $\Omega_R = 2\pi \times (130.7 \pm 0.2)$ kHz. The phase lock setup can be used for further experiments where phase coherence is needed. The lock quality for beat frequencies above 1 GHz is satisfactory with over 80% of power in the carrier, however below it might not be sufficient and other methods may have to be employed, if this range is needed. Note that the spectra were taken with a resolution bandwidth of 10 kHz. The actual percentage of power in the carrier might be a bit smaller than our calculated values.

The current setup is not yet optimal, there is still room for improvement. Our measured Rabi frequency of 130 kHz is well below the theoretically expected of 13 MHz. The reason for this is that we do not hit the atoms with beam center. An increase in Rabi frequency can also be achieved by increasing the power, but a smaller waist is more efficient since the intensity goes linearly with the power but anti proportional to square of the waist. An increase in the intensity would not change the β factor. One might therefore think there is no benefit in doing so. However, if the Rabi frequency is sufficiently high, not only a quick population transfer can be achieved but the influence of magnetic field fluctuations can also be overcome and thus the influence of one decoherence source is reduced.

We phase-locked the DL pro to the free running DL 100. Hence the latter has no stable frequency. Let us assume that the DL 100 has a small frequency shift δf. To ensure a stable frequency difference, the phase lock now reacts by regulating the DL pro and shifting its frequency by the same amount. The beat signal is therefore stable but frequency fluctuations of the DL100 directly translate into fluctuations of detuning $\delta f = \delta\Delta$, which in turn lead to an unstable Rabi frequency. An additional frequency stabilization of the DL 100 would solve this problem.

The fluctuations in power of the lasers were also not taken care of; a lack of stabilization leads to intensity fluctuations which, due to (2.8), also lead to an unstable Rabi frequency. An additional AOM in the second part of the setup, which is used to stabilize power, would solve this problem.

The relative contribution of incoherent background to inelastic scattering rate can be measured as described in section 5.1.

Bibliography

[1] Nils Pehoviak. Laserstabilisierung durch Modulationstransferspektroskopie in ^{6}Li. *Bachelor thesis, University of Heidelberg*, 2013.

[2] Paul Hill. Implementation of a Versitile Optical Phase Locked Loop for Experiments with Ultracold Lithium. *Bachelor thesis, University of Heidelberg*, 2018.

[3] Ralf Klemt. Many-body correlations in a quasi-two-dimensional, ultracold atomic Fermi gas. *Master thesis. Heidelberg University*, 2016.

[4] Sebastian Blänsdorf. Light-induced nuclear spin-flips in ^{6}Li ground states through Raman-transitions. *Bachelor thesis, University of Heidelberg*, 2018.

[5] Tony Hubert. Stimulated Raman transitions between hyperfine ground states of magnetically trapped rubidium-87 atoms. *Msc., University of Amsterdam*, 2015.

[6] Christopher J Foot et al. *Atomic physics*, volume 7. Oxford University Press, 2005.

[7] Michael E Gehm. Properties of 6Li. *Jetlab,*, 2003.

[8] Ran Wei and Erich J. Mueller. Magnetic-field dependence of Raman coupling in alkali-metal atoms. *Phys. Rev. A*, 87:042514, Apr 2013.

[9] Daniel A Steck. Rubidium 87 D line data, 2001.

[10] Roland E Best. *Phase-locked loops: design, simulation, and applications*. McGraw-Hill Education, 2007.

[11] Toptica Photonics. Scientific lasers, https://www.toptica.com/fileadmin/editors_english/11_brochures_datasheets/01_brochures/toptica_br_scientific_lasers.pdf, Visited: 14.04.2021.

[12] Melanie Müller. Realization and characterization of a phase locker laser system for coherent spectroscopy of fiber-coupled cesium atoms. *Diplomski rad. Mainz, Johannes Gutenberg Universität-Institut für Physik*, 2010.

[13] Tobias Müther. *Evaporative Kühlung in optischen Dipolpotentialen*. PhD thesis, Hannover: Universität, 2005.

[14] Harold J Metcalf and Peter Van der Straten. Laser cooling and trapping of neutral atoms. *The Optics Encyclopedia: Basic Foundations and Practical Applications*, 2007.

[15] Timo Bastian Ottenstein. *Few-body physics in ultracold Fermi gases*. PhD thesis, Ruprecht-Karls Universität Heidelberg, 2010.

[16] Gerhard Zürn. *Few-fermion systems in one dimension*. PhD thesis, 2012.

[17] JHW Becher. Towards Spin and Site-resolved, Single-Atom Imaging of 6Li Atoms in a Multiwell Potential. *Masters's thesis. Heidelberg University*, 2016.

[18] Andrea Bergschneider. *Strong correlations in few-fermion systems*. PhD thesis, 2017.

[19] Rudolf Grimm, Matthias Weidemüller, and Yurii B Ovchinnikov. Optical dipole traps for neutral atoms. *Advances in atomic, molecular, and optical physics*, 42:95–170, 2000.

[20] Dipankar Das and Vasant Natarajan. Absolute frequency measurement of the lithium D lines: Precise determination of isotope shifts and fine-structure intervals. *Phys. Rev. A*, 75:052508, May 2007.

Danksagung

An dieser Stelle möchte ich jenen danken, die zum Gelingen dieser Arbeit beigetragen haben.
Zuerst Selim, dafür mir die Arbeit in der Gruppe angeboten zu haben und für seine immer freundliche und hilfsbereite Art.
Ganz besonders möchte ich mich bei Philipp bedanken, dafür mir das Arbeiten im Labor von Grund auf beigebracht zu haben, für das geduldsame und ausführliche Beantworten meiner vielen Fragen und das Korrekturlesen. Bei Problemen aller Art konnte ich immer auf seine Hilfe zählen.
Meiner Familie und meiner Freundin danke ich für die ständige Unterstützung, ohne die das Studium nicht möglich gewesen wäre.

Finally I want to thank the readers of this thesis for their interest.

Erklärung

Ich erkläre, dass ich die Arbeit selbstständig angefertigt und nur die angegebenen Hilfsmittel benutzt habe. Alle Stellen, die dem Wortlaut oder dem Sinne nach anderen Werken, gegebenenfalls auch elektronischen Medien, entnommen sind, sind von mir durch Angabe der Quelle und des Zugriffsdatums sowie dem Ausdruck der ersten Seite belegt; sie liegen zudem für den Zeitraum von 2 Jahren entweder auf einem elektronischen Speichermedium im PDF-Format oder in gedruckter Form vor.

Heidelberg, den 15.04.2021

.....
Nilab Abbas